Supporting Information (SI)

Quaternary Ru(II) Complexes of Terpyridines, Saccharin and 1, 2-Azoles: Effect of Substituents on Molecular Structure, Speciation, Photoactivity, and Cytotoxicity

Priyaranjan Kumar[a], Prerana Singh[bc], Sanjoy Saren[a], Juhi Sayala [a], Sri Sivakumar[b], Ashis K. Patra*[a]

Author address: [a]Department of Chemistry, Indian Institute of Technology Kanpur, Kanpur 208016, Uttar Pradesh, India. E-mail: akpatra@iitk.ac.in

[b]Department of Chemical Engineering, DST Thematic Unit of Excellence on Soft Nanofabrication, Indian Institute of Technology Kanpur, Kanpur 208016, Uttar Pradesh, India.

[c]Department of Biological Sciences & Bioengineering, Indian Institute of Technology Kanpur, Uttar Pradesh 208016, India

Contents

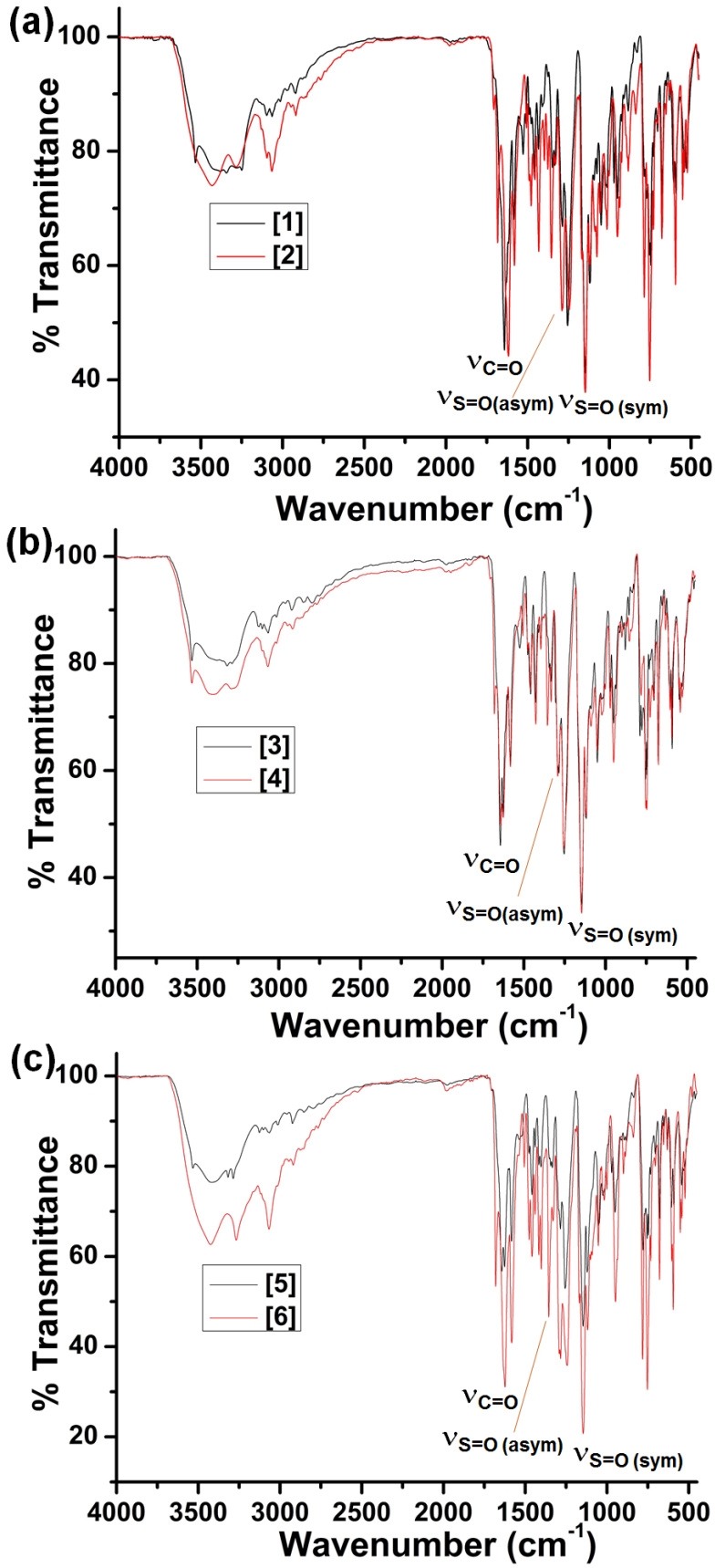

Fig. S1. Overlay of solid-state FTIR spectra (in KBr Pellets) of the complexes (a) **1** and **2**; (b) **3** and **4** and (c) **5** and **6**.

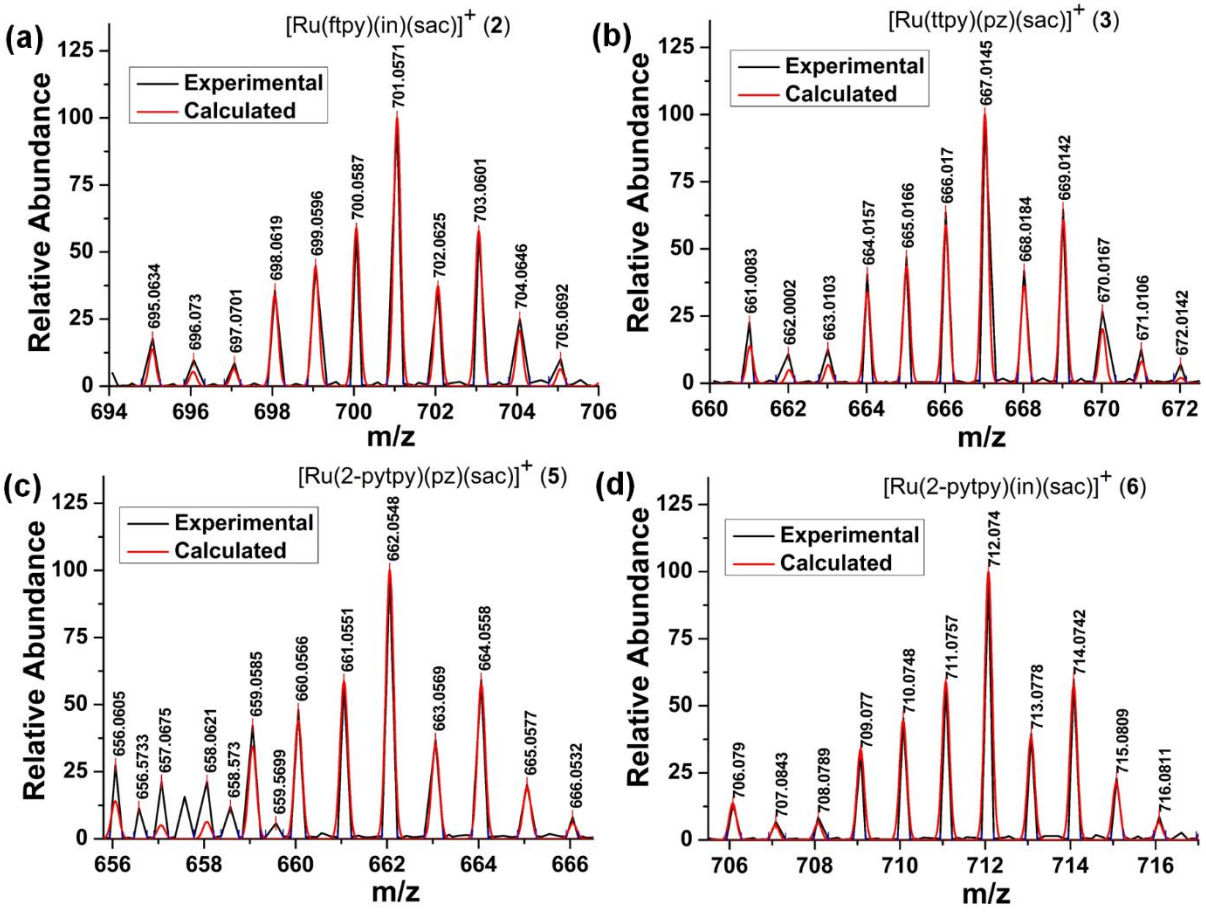

Fig. S2. ESI-MS spectra of the complexes in methanol. An overlay of calculated (red) and experimental (black) isotopic distribution pattern of complexes (a) **2**; (b) **3**; (c) **5** and (d) **6**.

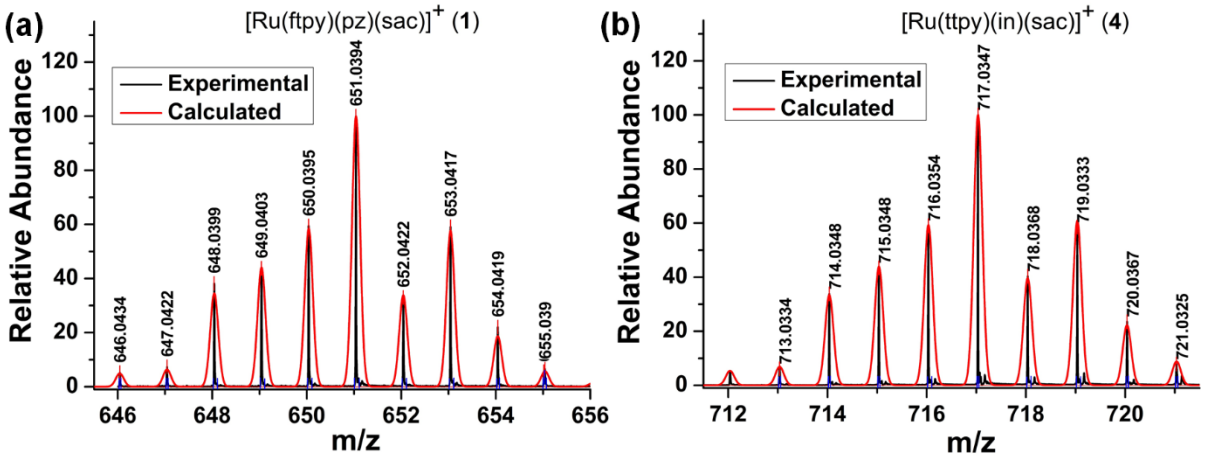

Fig. S3. ESI-MS spectra of the complexes in methanol. An overlay of calculated (red) and experimental (black) isotopic distribution pattern of complexes (a) **1** and (b) **4**.

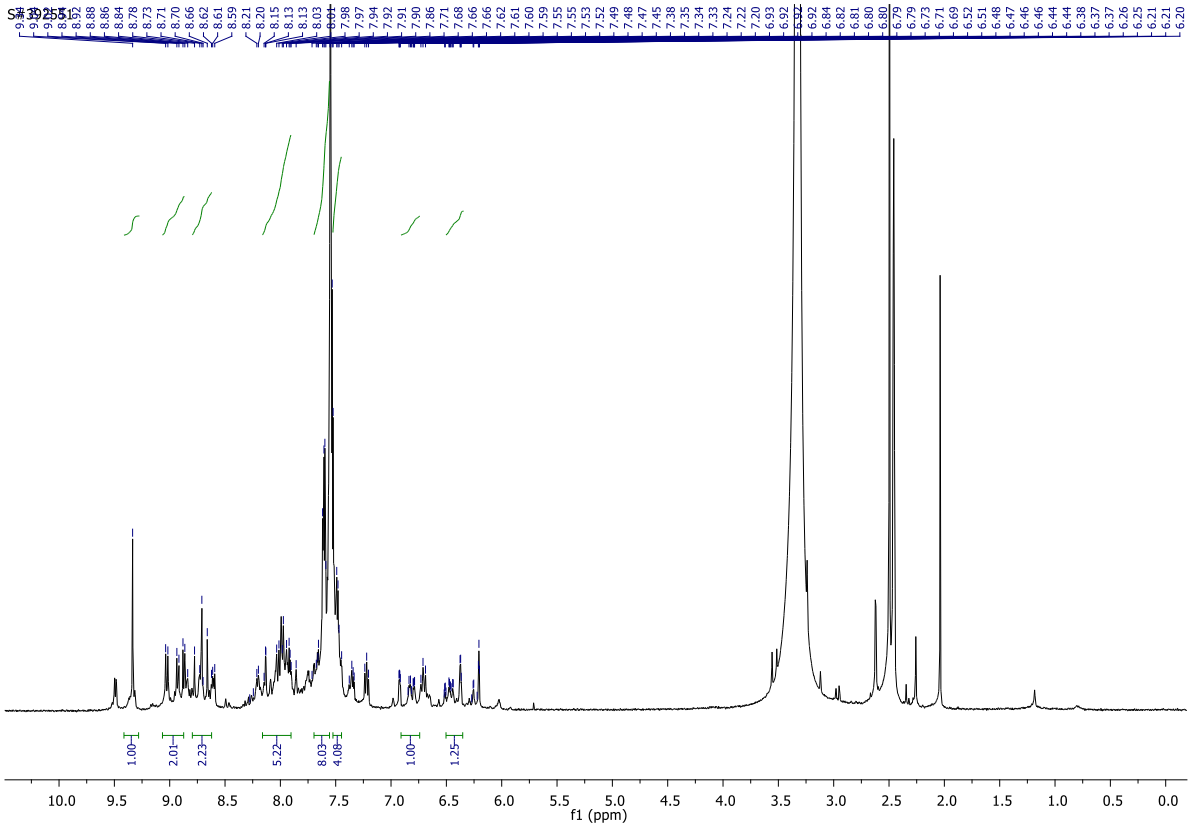

Fig. S4. ^{1}H-NMR (400 MHz, DMSO-d_6) spectra of complex **1** at 298 K.

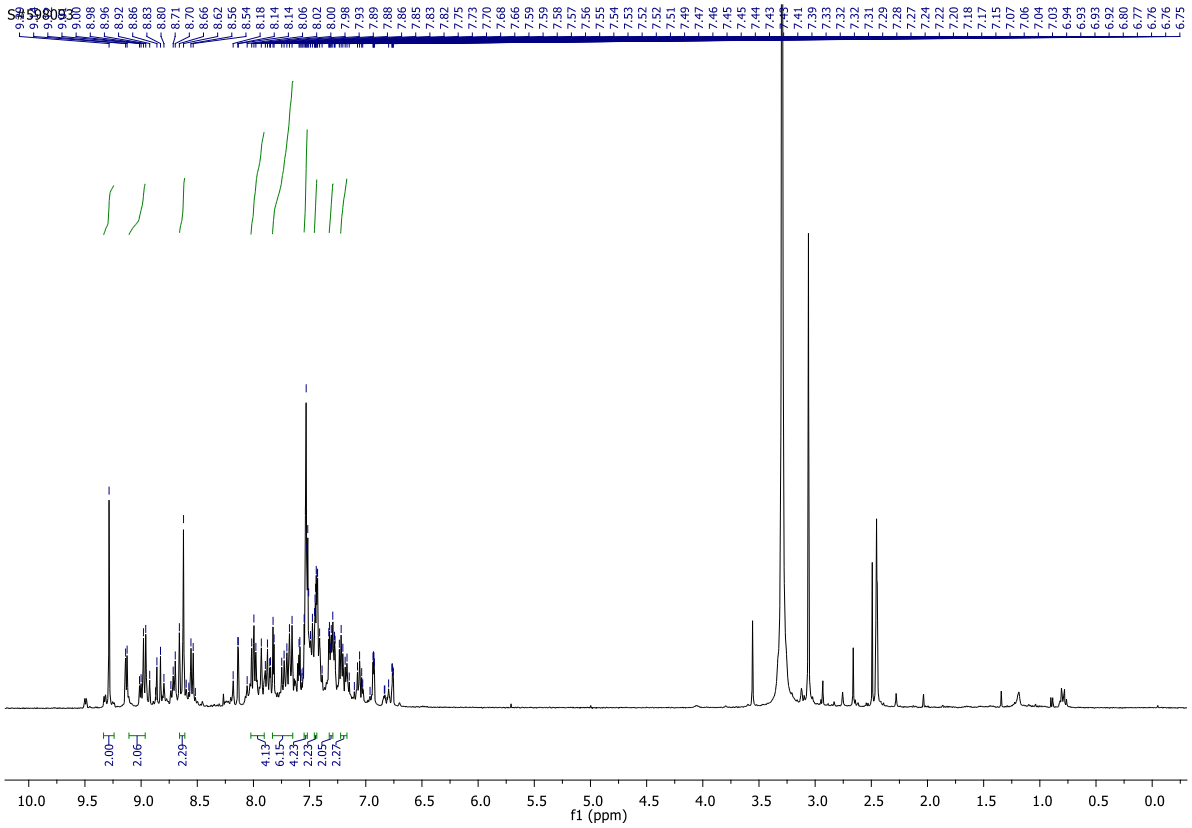

Fig. S5. ^{1}H-NMR (400 MHz, DMSO-d_6) spectra of complex **2** at 298 K.

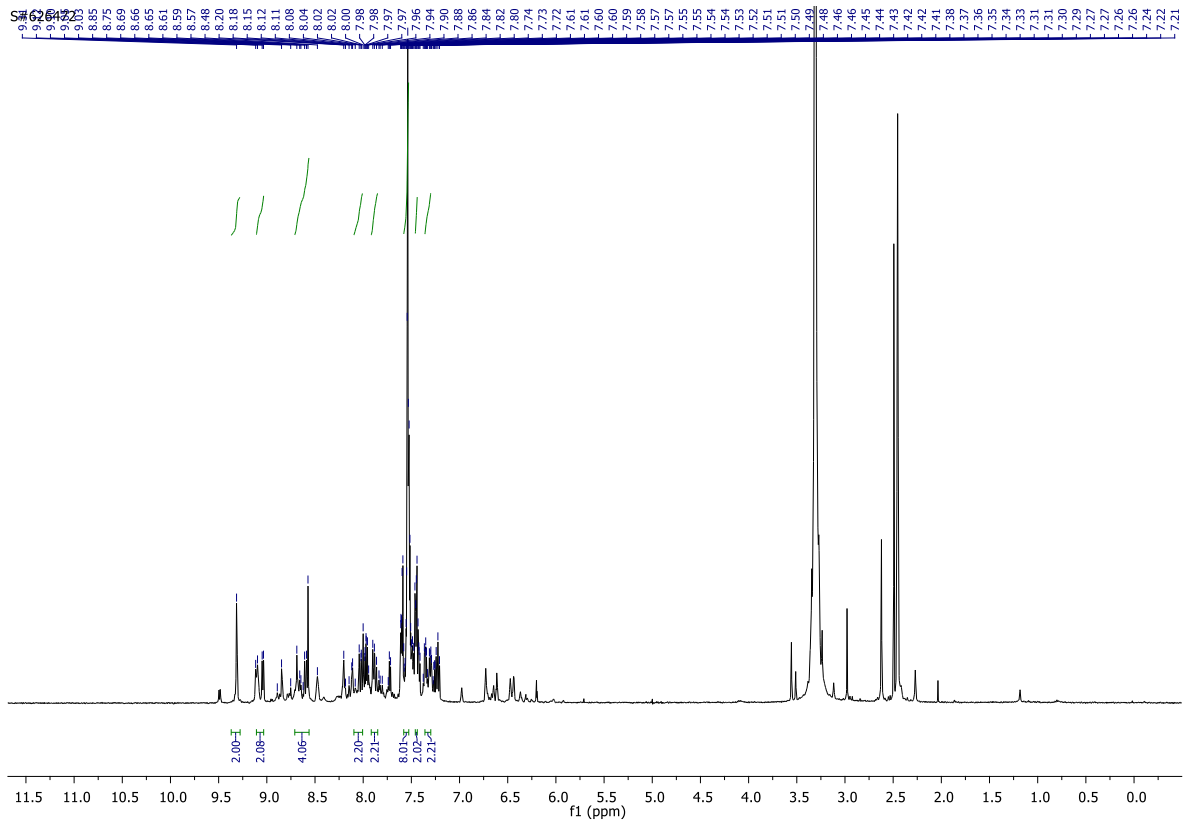

Fig. S6. ^{1}H-NMR (400 MHz, DMSO-d_6) spectra of complex **3** at 298 K.

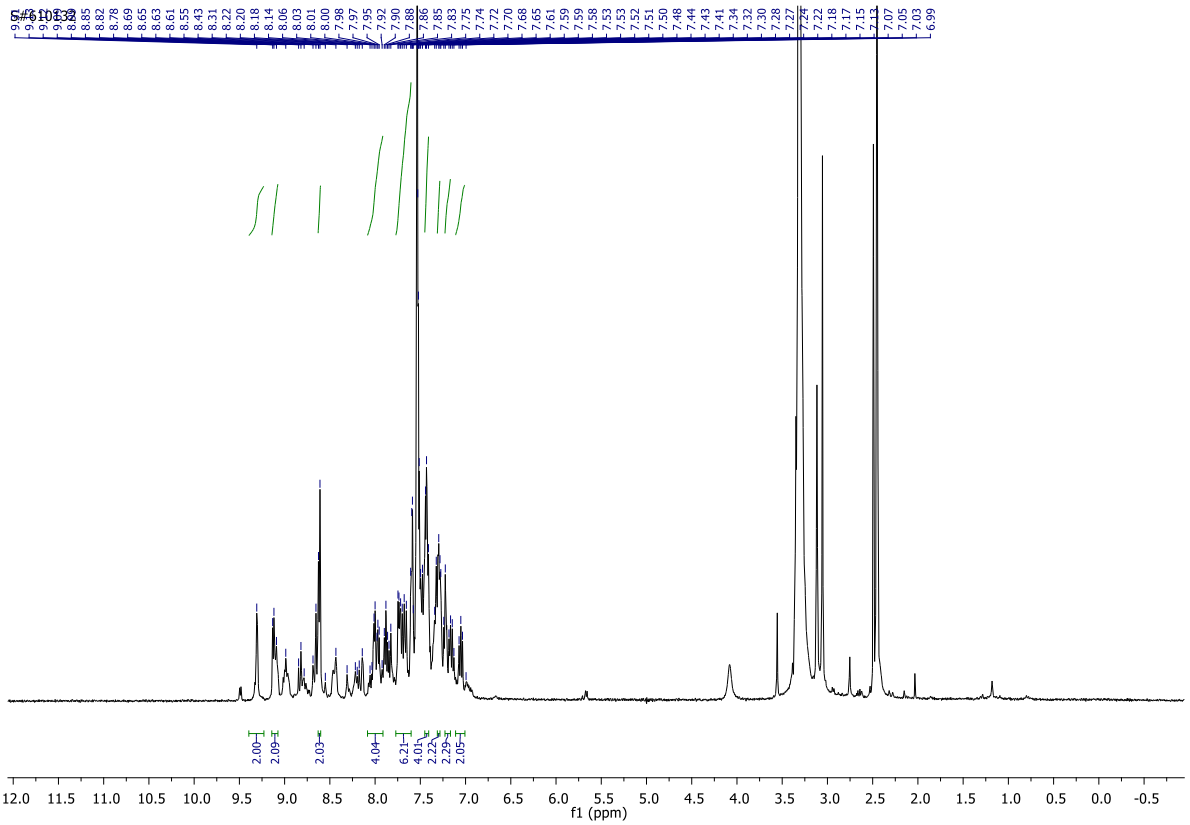

Fig. S7. ^{1}H-NMR (400 MHz, DMSO-d_6) spectra of complex **4** at 298 K.

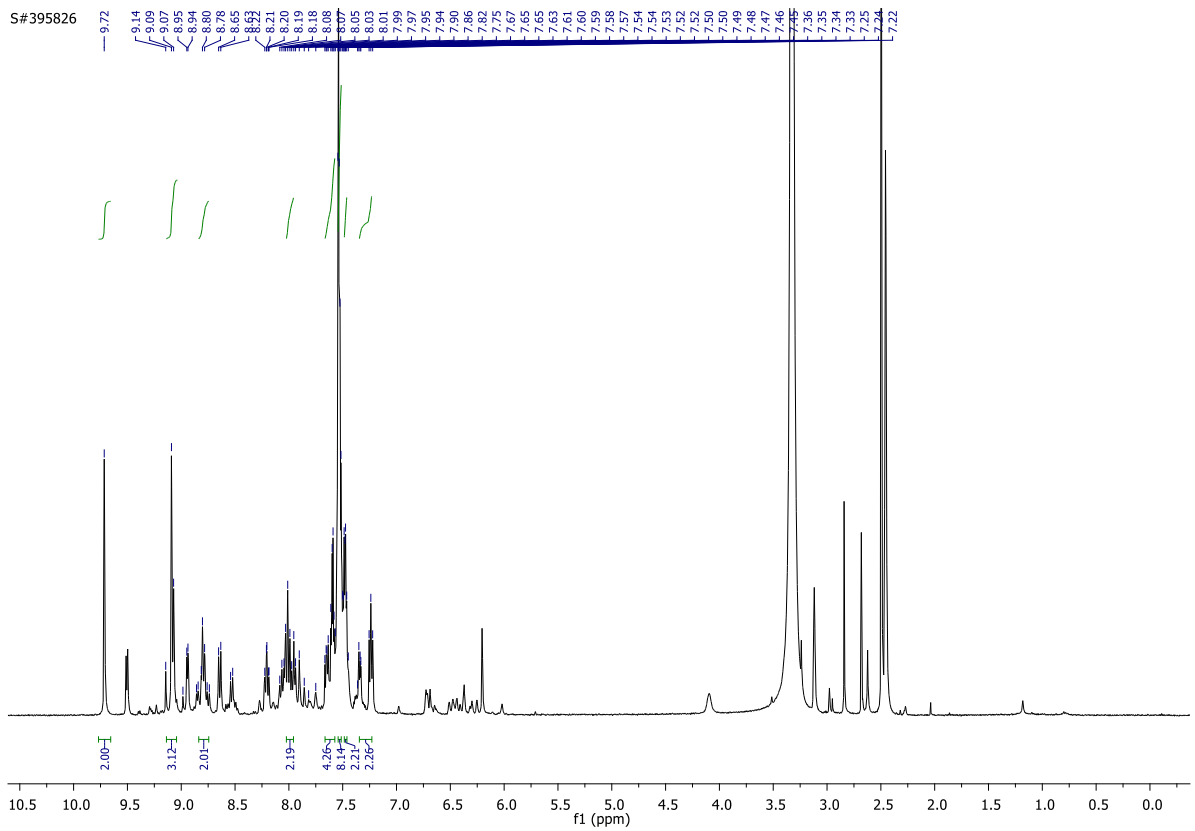

Fig. S8. [1]H-NMR (400 MHz, DMSO-d_6) spectra of complex **5** at 298 K.

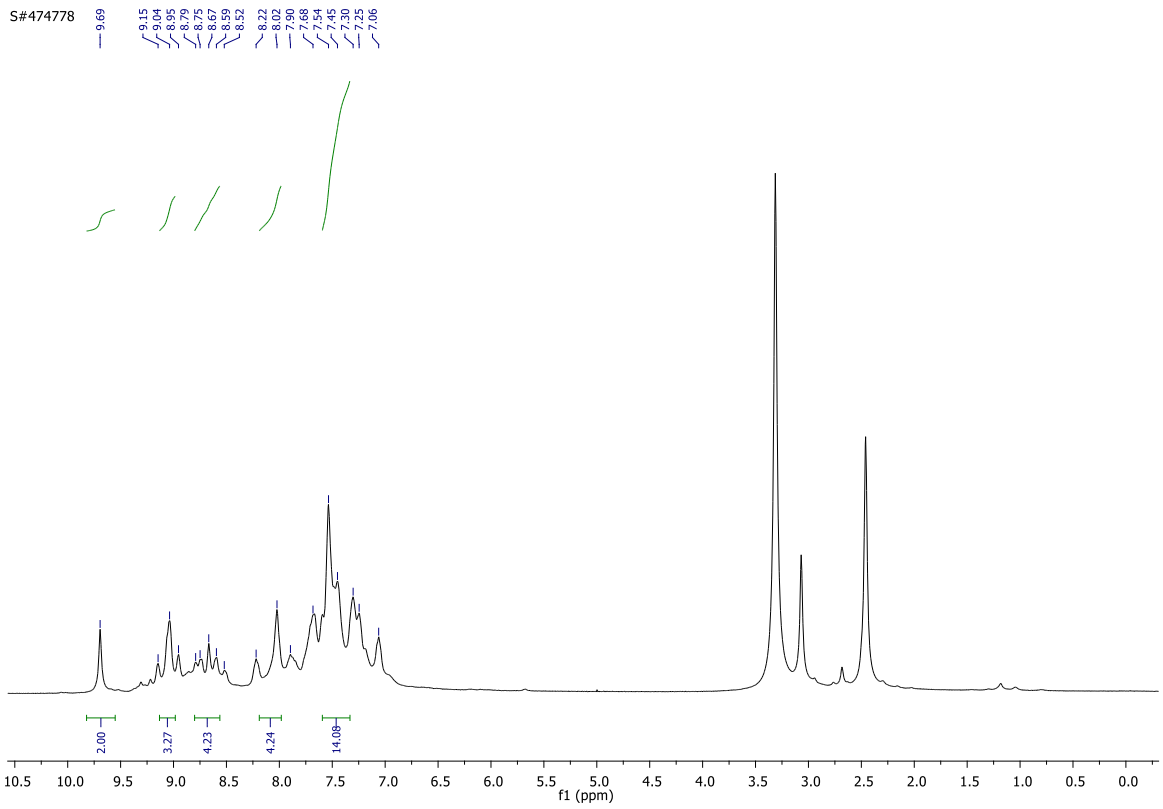

Fig. S9. [1]H-NMR (400 MHz, DMSO-d_6) spectra of complex **6** at 298 K.

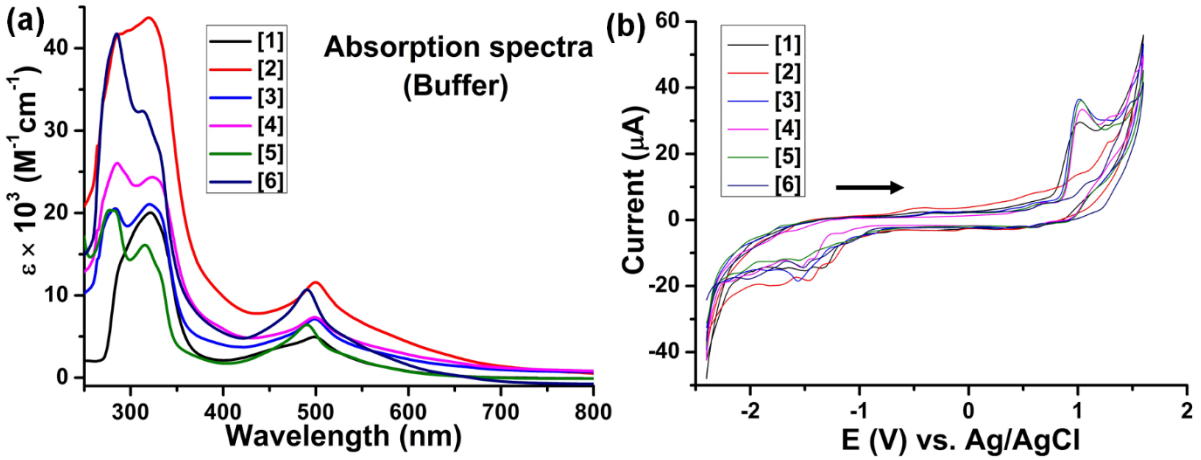

Fig. S10. (a) An overlay of UV-Vis spectra of the complexes **1–6** (20 μM) in 1% (v/v) DMF–5 mM Tris-HCl/NaCl buffer (pH = 7.2). (b) Cyclic voltammogram overlay of the complexes **1–6** (1 mM) with scan rate 50 mVs^{-1} in DMF with 0.1 M $^{n}Bu_4NClO_4$ supporting electrolyte.

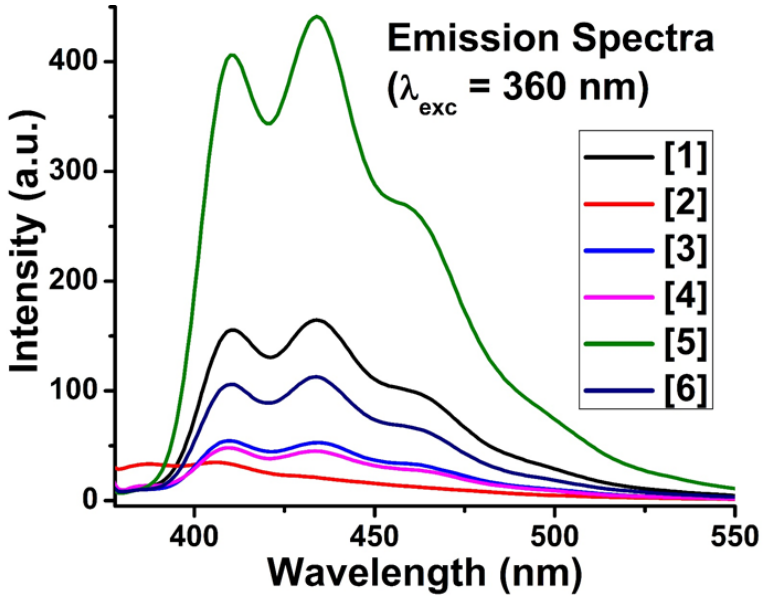

Fig. S11. Fluorescence spectral overlay (λ_{ex} = 360 nm) of the complexes **1–6** (10 μM) in DMF.

Table S1. Selected crystallographic data and structure refinement parameters for complexes **1, 2** and **3**.

Parameters	**1**	**2**	**3**
Empirical formula	$C_{35.96}H_{24.9}N_7O_{6.98}RuS_2$	$C_{40}H_{27}N_7O_7RuS_2$	$C_{36}H_{24}N_7O_6RuS_3$
M_r	831.49	882.87	847.87
Crystal system	Triclinic	Triclinic	Orthorhombic
Space group	*P-1*	*P-1*	*Pbca*
a(Å)	11.7775(8)	12.3256(13)	11.9146(5)
b(Å)	13.4849(9)	12.6904(14)	16.9265(7)
c (Å)	14.2982(9)	13.5220(13)	32.3157(13)
α (deg)	105.076(2)	82.577(4)	90. 000
b(deg)	114.080(2)	77.715(4)	90. 000
g(deg)	92.307(2)	61.308(4)	90. 000
Volume ($Å^3$)	1974.1(2)	1812.0(3)	6517.2(5)
Z	2	2	8
$\rho_{calc}g/cm^3$	1.399	1.618	1.728
μ (mm^{-1})	0.557	0.612	0.736
F(000)	843.0	896.0	3432.0
*T(*K)	273.15	100(2)	100(2)
2θ range for data collection(deg)	5.986 to 56.734	6.17 to 50.134	5.638 to 50.096
Limiting indices	$-15 \le h \le 15$, $-17 \le k \le 18$, $-19 \le l \le 19$	$-14 \le h \le 14$, $-15 \le k \le 15$, $-16 \le l \le 16$	$-14 \le h \le 14$, $-20 \le k \le 20$, $-38 \le l \le 38$
Reflections collected	30386	21668	100979
Unique reflections	9791	6384	5764
R_{int}	0.0881	0.1118	0.1008
T_{min}/T_{max}	0.885/0.905	0.874/0.896	0.838/0.857
Data/restraints/parameters	9791/45/514	6384/0/514	5764/0/480
GOF on F^2	1.010	1.055	1.093
R_1[a] and wR_2[b] [$I>2\sigma(I)$]	R_1 = 0.0671, wR_2 = 0.1610	R_1 = 0.0729, wR_2 = 0.1299	R_1 = 0.0387, wR_2 = 0.0833
R_1 and wR_2 (all data)	R_1 = 0.1093, wR_2 = 0.1826	R_1 = 0.1124, wR_2 = 0.1443	R_1 = 0.0554, wR_2 = 0.0936
Largest diff. peak/hole ($eÅ^{-3}$)	2.29/-1.32	1.19/-0.69	0.95/-0.59
CCDC deposition serial number	2096938	2096939	2096940

[a] $R_1 = \Sigma||F_o|-|F_c||/\Sigma|F_o|$; [b] $wR_2 = \{\Sigma[w(F_o^2-F_c^2)^2]/\Sigma[w(F_o^2)^2]\}^{1/2}$. Goodness-of-fit (GOF) = $\{\Sigma[w(F_o^2-F_c^2)^2/(n-p)]\}^{1/2}$, where n = number of data and p = number of parameters refined.

Table S2. Selected crystallographic data and structure refinement parameters for the complexes **4**, **5** and **6**.

Parameters	**4**	**5**	**6**
Empirical formula	$C_{40}H_{26}N_7O_6RuS_3$	$C_{37}H_{26}N_8O_6RuS_2$	$C_{41}H_{28}N_8O_6RuS_2$
M_r	897.93	843.85	893.90
Crystal system	Triclinic	Triclinic	Triclinic
Space group	P-1	P-1	P-1
a (Å)	12.0404(8)	9.8383(4)	12.4757(5)
b (Å)	14.6966(11)	11.6116(5)	12.9156(5)
c (Å)	14.9939(10)	16.4777(7)	13.4640(5)
α (deg)	105.898(2)	83.7270(10)	86.0730(10)
b(deg)	101.054(2)	85.1190(10)	78.2220(10)
γ (deg)	111.592(2)	73.6830(10)	61.2780(10)
Volume (Å^3)	2242.1(3)	1792.83(13)	1861.38(13)
Z	2	2	2
ρ_{calc} (g/cm^3)	1.330	1.563	1.595
μ (mm^{-1})	0.539	0.613	0.596
F(000)	910.0	856.0	908.0
*T(*K)	100(2)	273(2)	100(2)
2θ range for data collection(deg)	4.82 to 50.1	4.842 to 50.09	6.186 to 56.674
Limiting indices	-14 ≤ h ≤ 14, -17 ≤ k ≤ 17, -17 ≤ l ≤ 17	-11 ≤ h ≤ 11, -13 ≤ k ≤ 13, -19 ≤ l ≤ 19	-16 ≤ h ≤ 16, -17 ≤ k ≤ 17, -17 ≤ l ≤ 17
Reflections collected	27350	21914	29267
Unique reflections	7926	6333	9250
R_{int}	0.0698	0.0485	0.0306
T_{min}/T_{max}	0.898/0.917	0.863/0.896	0.867/0.888
Data/restraints/parameters	7926/3/466	6333/0/484	9250/0/523
GOF on F^2	1.067	1.026	1.049
R_1[a] and wR_2[b] [$I>2\sigma(I)$]	R_1 = 0.0706, wR_2 = 0.1851	R_1 = 0.0378, wR_2 = 0.0845	R_1 = 0.0337, wR_2 = 0.0830
R_1 and wR_2 (all data)	R_1 = 0.0922, wR_2 = 0.2043	R_1 = 0.0502, wR_2 = 0.0898	R_1 = 0.0430, wR_2 = 0.0894
Largest diff. peak/hole (eÅ^{-3})	3.96/-2.09	0.94/-0.94	0.71/-0.80
CCDC deposition serial number	2096941	2096942	2096943

[a]$R_1 = \Sigma||F_o|-|F_c||/\Sigma|F_o|$; [b]$wR_2 = \{\Sigma[w(F_o^2-F_c^2)^2]/\Sigma[w(F_o^2)^2]\}^{1/2}$. Goodness-of-fit (GOF) = $\{\Sigma[w(F_o^2-F_c^2)^2/(n-p)]\}^{1/2}$, where n = number of data and p = number of parameters refined.

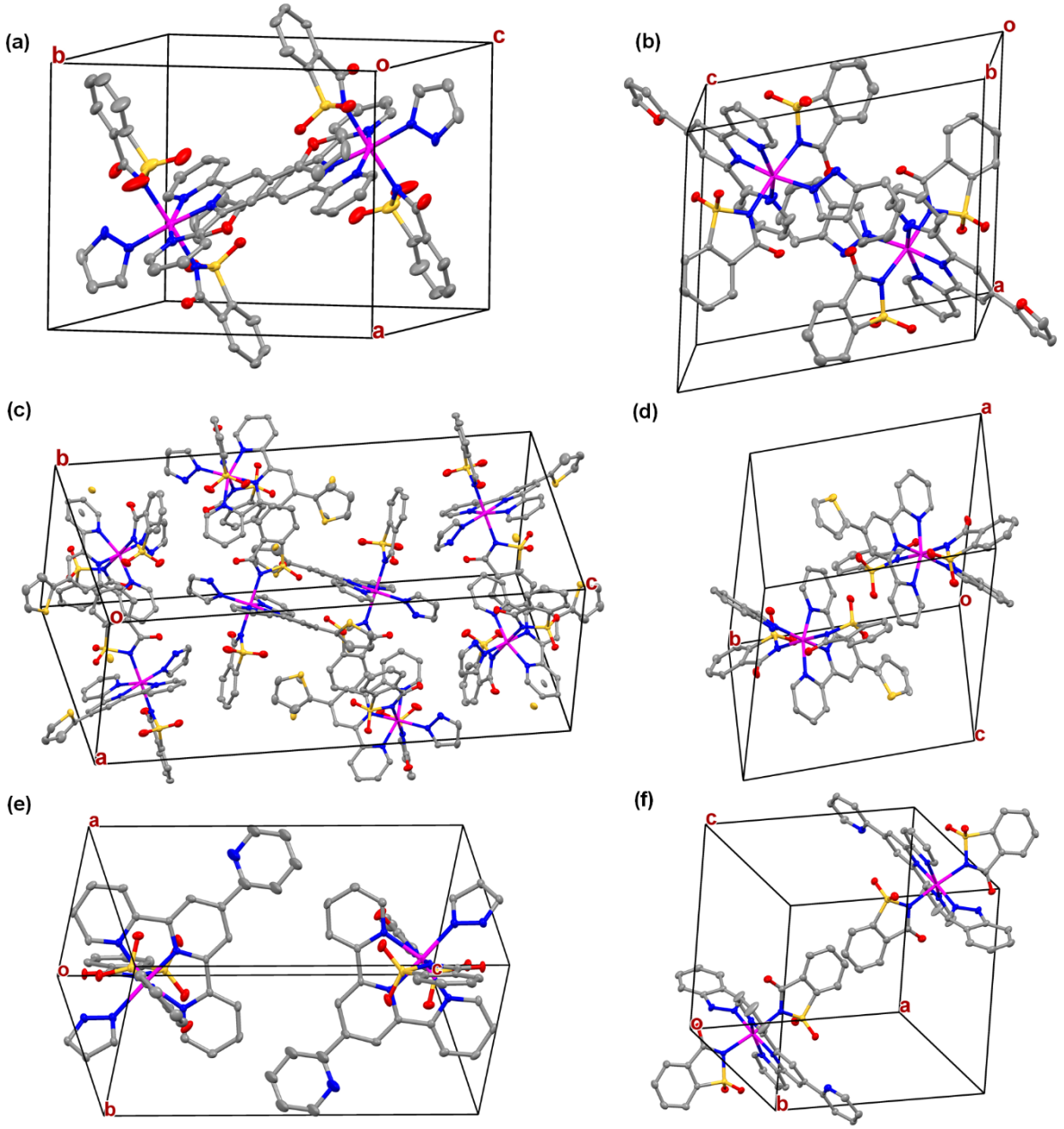

Fig. S12. Unit cell diagram of the complexes (a) **1**; (b) **2**; (c) **3**; (d) **4**; (e) **5** and (f) **6.**

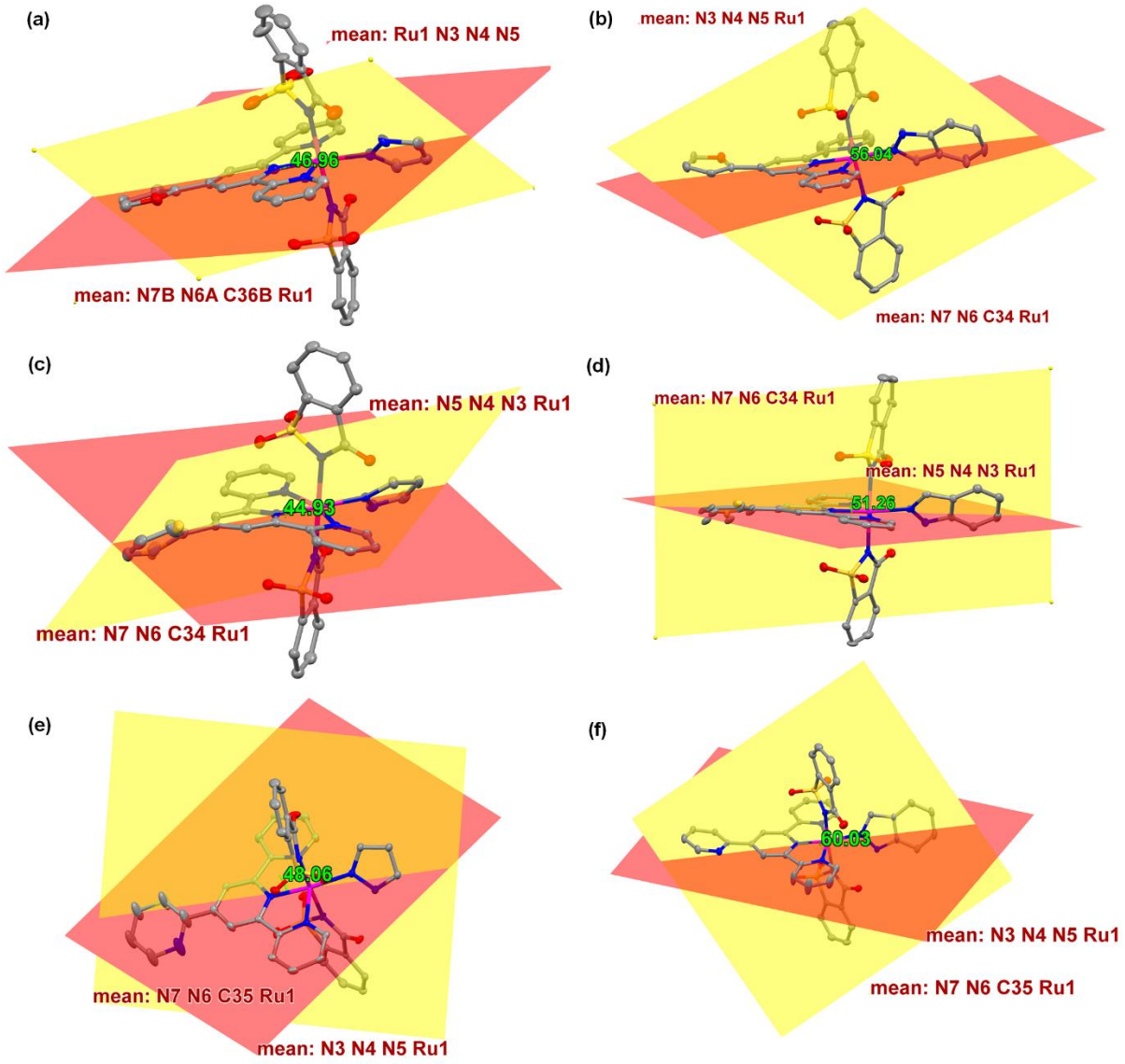

Fig. S13. Dihedral angle between the planes of R-tpy and 1, 2 azoles containing Ru-centre (a) **1**; (b) **2**; (c) **3**; (d) **4**; (e) **5** and (f) **6.**

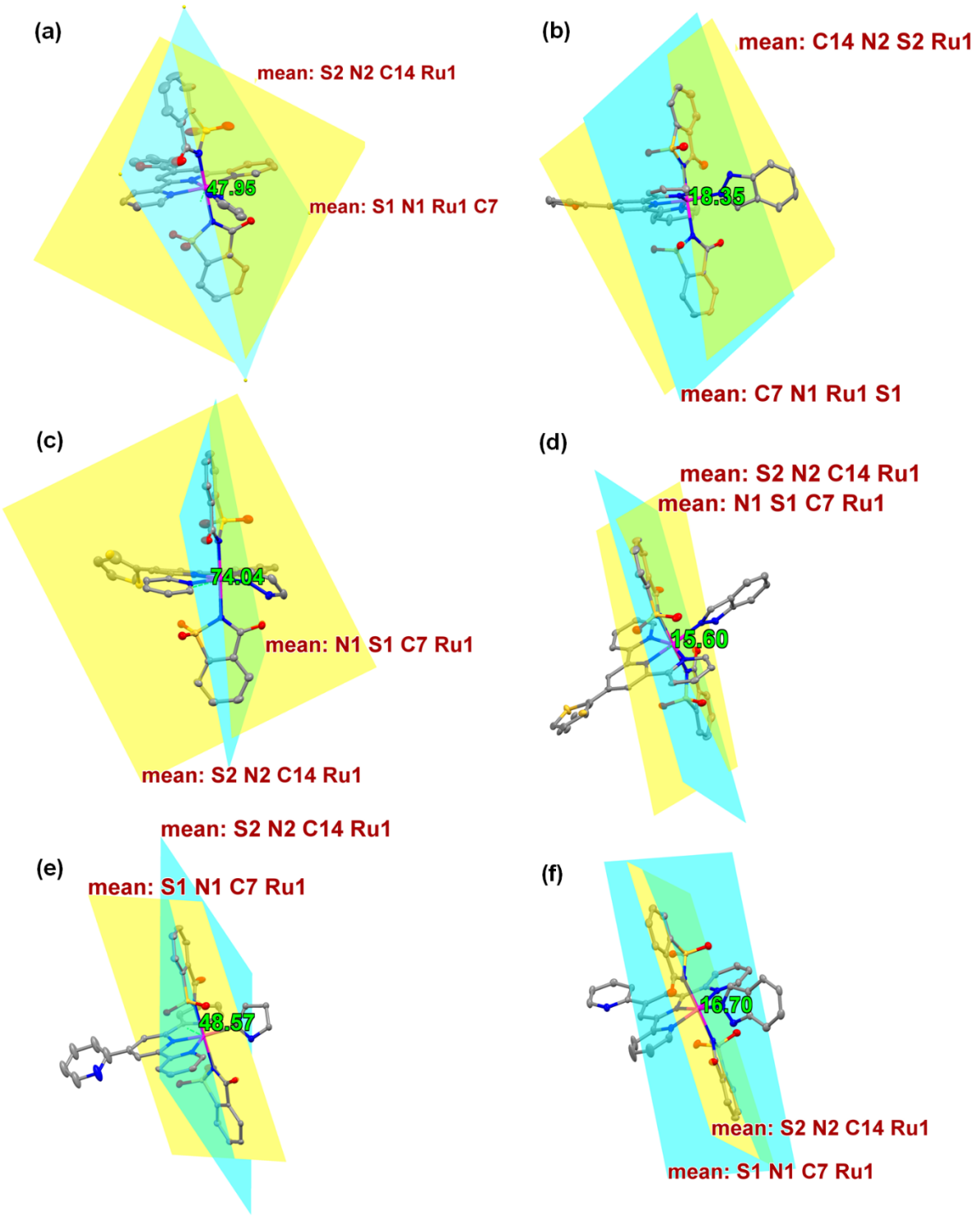

Fig. S14. Dihedral angle between the planes of sac and sac containing Ru centre (a) **1**; (b) **2**; (c) **3**; (d) **4**; (e) **5** and (f) **6**.

Table S3. Selected bond lengths and bond angles obtained from the X-ray structures of the complexes **1** and **2**.

Bond lengths (Å) (**1**)		Bond lengths (Å) (**2**)	
Ru1-N3	2.084(4)	Ru1-N6	2.110(5)
Ru1-N5	2.069(4)	Ru1-N2	2.159(6)
Ru1-N4	1.942(4)	Ru1-N3	2.084(6)
Ru1-N2	2.141(4)	Ru1-N1	2.115(6)
Ru1-N1	2.138(4)	Ru1-N5	2.065(5)
Ru1-N6A	2.107(5)	Ru1-N4	1.932(6)
Ru1-N6B	2.117(10)		
Bond Angles (deg)		**Bond Angles (deg)**	
N3-Ru1-N2	92.82(14)	N5-Ru1-N2	92.4(2)
N3-Ru1-N1	87.39(15)	N5-Ru1-N1	84.8(2)
N3-Ru1-N6A	99.9(3)	N3-Ru1-N6	106.0(2)
N3-Ru1-N6B	101.2(4)	N3-Ru1-N2	86.9(2)
N5-Ru1-N3	159.07(16)	N3-Ru1-N1	89.1(2)
N5-Ru1-N2	89.57(14)	N1-Ru1-N2	174.3(2)
N5-Ru1-N1	90.96(15)	N5-Ru1-N6	95.3(2)
N5-Ru1-N6A	101.0(3)	N5-Ru1-N2	92.6(2)
N5-Ru1-N6B	99.7(4)	N5-Ru1-N3	158.7(2)
N4-Ru1-N3	79.21(15)	N5-Ru1-N1	92.7(2)
N4-Ru1-N5	80.00(16)	N4-Ru1-N6	172.8(3)
N4-Ru1-N2	89.82(15)	N4-Ru1-N2	93.1(2)
N4-Ru1-N1	92.19(15)	N4-Ru1-N3	78.8(3)
N4-Ru1-N6A	175.3(3)	N4-Ru1-N1	90.0(2)
N4-Ru1-N6B	178.9(4)	N4-Ru1-N5	79.9(2)
N1-Ru1-N2	177.98(15)		
N6A-Ru1-N2	85.6(3)		
N6A-Ru1-N1	92.4(3)		
N6B-Ru1-N2	89.1(4)		
N6B-Ru1-N1	88.9(4)		

Table S4. Selected bond lengths and bond angles obtained from the X-ray structures of the complexes **3** and **4**.

Bond lengths (Å) (**3**)		Bond lengths (Å) (**4**)	
Ru1-N6	2.131(3)	Ru1-N3	2.082(5)
Ru1-N4	1.938(3)	Ru1-N6	2.123(6)
Ru1-N5	2.085(3)	Ru1-N4	1.954(6)
Ru1-N3	2.066(3)	Ru1-N2	2.155(6)
Ru1-N1	2.139(3)	Ru1-N5	2.087(6)
Ru1-N2	2.185(3)	Ru1-N1	2.128(6)
Bond Angles (deg)		**Bond Angles (deg)**	
N6-Ru1-N1	88.16(12)	N3-Ru1-N6	95.2(2)
N6-Ru1-N2	91.96(11)	N3-Ru1-N2	93.9(2)
N4-Ru1-N6	177.98(13)	N3-Ru1-N1	92.8(2)
N4-Ru1-N5	79.51(12)	N6-Ru1-N2	92.6(2)
N4-Ru1-N3	79.81(12)	N6-Ru1-N1	84.3(2)
N4-Ru1-N1	89.84(12)	N4-Ru1-N3	79.3(2)
N4-Ru1-N2	90.03(12)	N4-Ru1-N6	172.4(2)
N5-Ru1-N6	100.90(12)	N4-Ru1-N2	92.9(2)
N5-Ru1-N1	93.63(12)	N4-Ru1-N5	78.9(2)
N5-Ru1-N2	87.64(12)	N4-Ru1-N1	90.7(2)
N3-Ru1-N6	99.81(12)	N5-Ru1-N3	158.2(2)
N3-Ru1-N5	159.29(12)	N5-Ru1-N6	106.6(2)
N3-Ru1-N1	87.49(12)	N5-Ru1-N2	86.3(2)
N3-Ru1-N2	91.19(11)	N5-Ru1-N1	89.3(2)
N1-Ru1-N2	178.68(12)	N1-Ru1-N2	173.7(2)

Table S5. Selected bond lengths and bond angles obtained from the X-ray structures of the complexes **5** and **6**.

Bond lengths (Å) (**5**)		Bond lengths (Å) (**6**)	
Ru1-N4	1.940(3)	Ru1-N4	1.9525(18)
Ru1-N2	2.138(2)	Ru1-N1	2.1219(19)
Ru1-N1	2.155(2)	Ru1-N2	2.1587(19)
Ru1-N5	2.091(3)	Ru1-N3	2.099(2)
Ru1-N3	2.068(3)	Ru1-N5	2.0767(19)
Ru1-N6	2.132(3)	Ru1-N6	2.1162(19)
Bond Angles (deg)		**Bond Angles (deg)**	
N4-Ru1-N2	89.95(10)	N4-Ru1-N1	90.59(7)
N4-Ru1-N1	91.67(10)	N4-Ru1-N2	92.36(7)
N4-Ru1-N5	79.50(10)	N4-Ru1-N3	79.09(7)
N4-Ru1-N3	79.84(10)	N4-Ru1-N5	79.64(7)
N4-Ru1-N6	174.38(10)	N4-Ru1-N6	173.14(8)
N2-Ru1-N1	177.90(9)	N1-Ru1-N2	175.26(7)
N5-Ru1-N2	92.77(9)	N3-Ru1-N1	90.09(8)
N5-Ru1-N1	86.22(10)	N3-Ru1-N2	86.83(7)
N5-Ru1-N6	102.66(10)	N3-Ru1-N6	105.93(7)
N3-Ru1-N2	90.20(10)	N5-Ru1-N1	91.82(7)
N3-Ru1-N1	91.39(10)	N5-Ru1-N2	92.36(7)
N3-Ru1-N5	159.12(10)	N5-Ru1-N3	158.66(7)
N3-Ru1-N6	98.19(10)	N5-Ru1-N6	95.41(7)
N6-Ru1-N2	84.78(10)	N6-Ru1-N1	84.80(7)
N6-Ru1-N1	93.64(10)	N6-Ru1-N2	92.58(7)

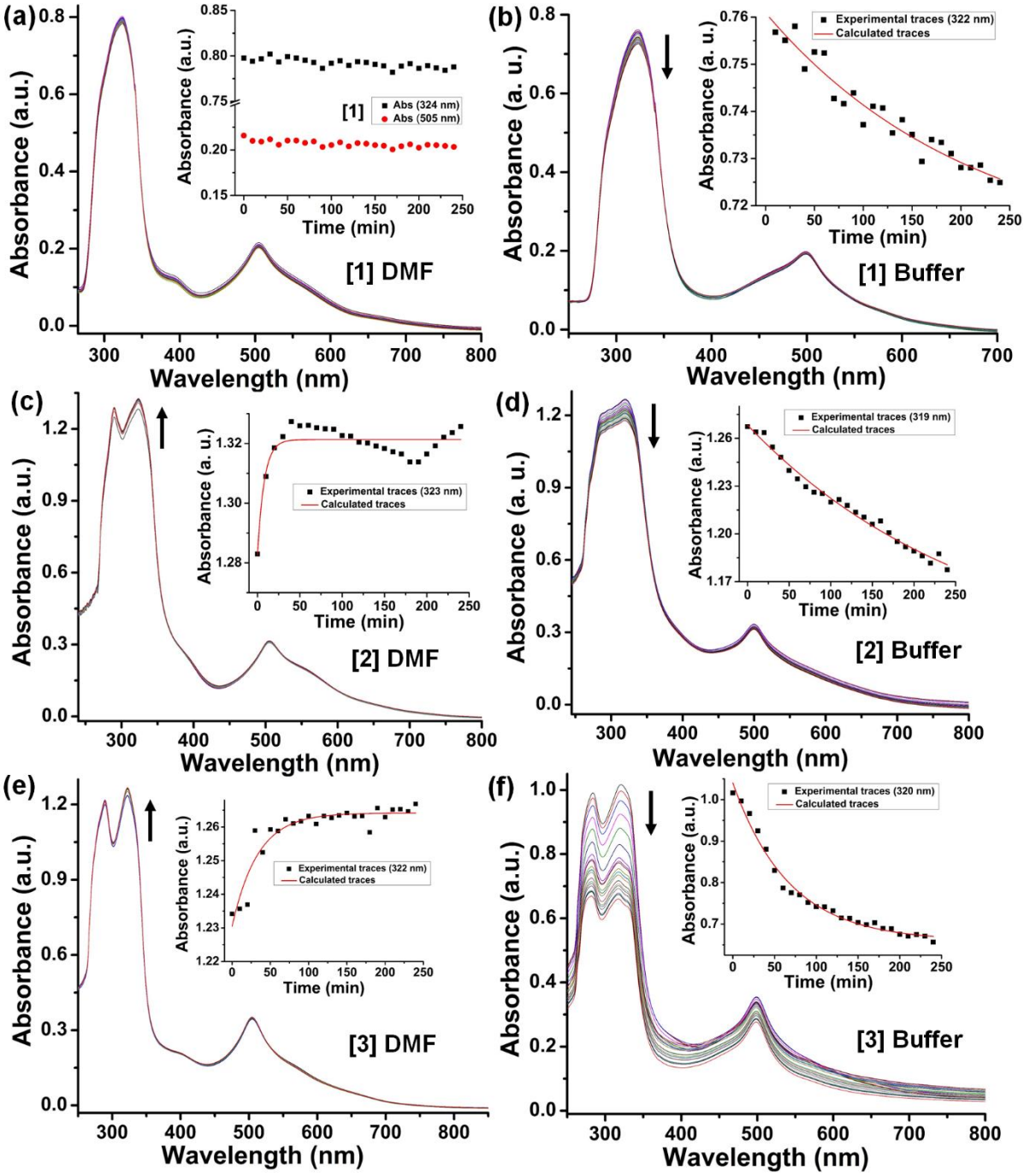

Fig. S15. Solvolysis of the complexes in DMF and in 2% (v/v) DMF–5 mM Tris-HCl/NaCl buffer (pH = 7.2) evident from concomitant changes in absorbance spectral profile at T = 298 K for 4 h. (a) **1** (39 μM) in DMF; (b) **1** (39 μM) in DMF–buffer; (c) **2** (30 μM) in DMF; (d) **2** (30 μM) in DMF–buffer; (e) **3** (49 μM) in DMF and (f) **3** (49 μM) in DMF–buffer.

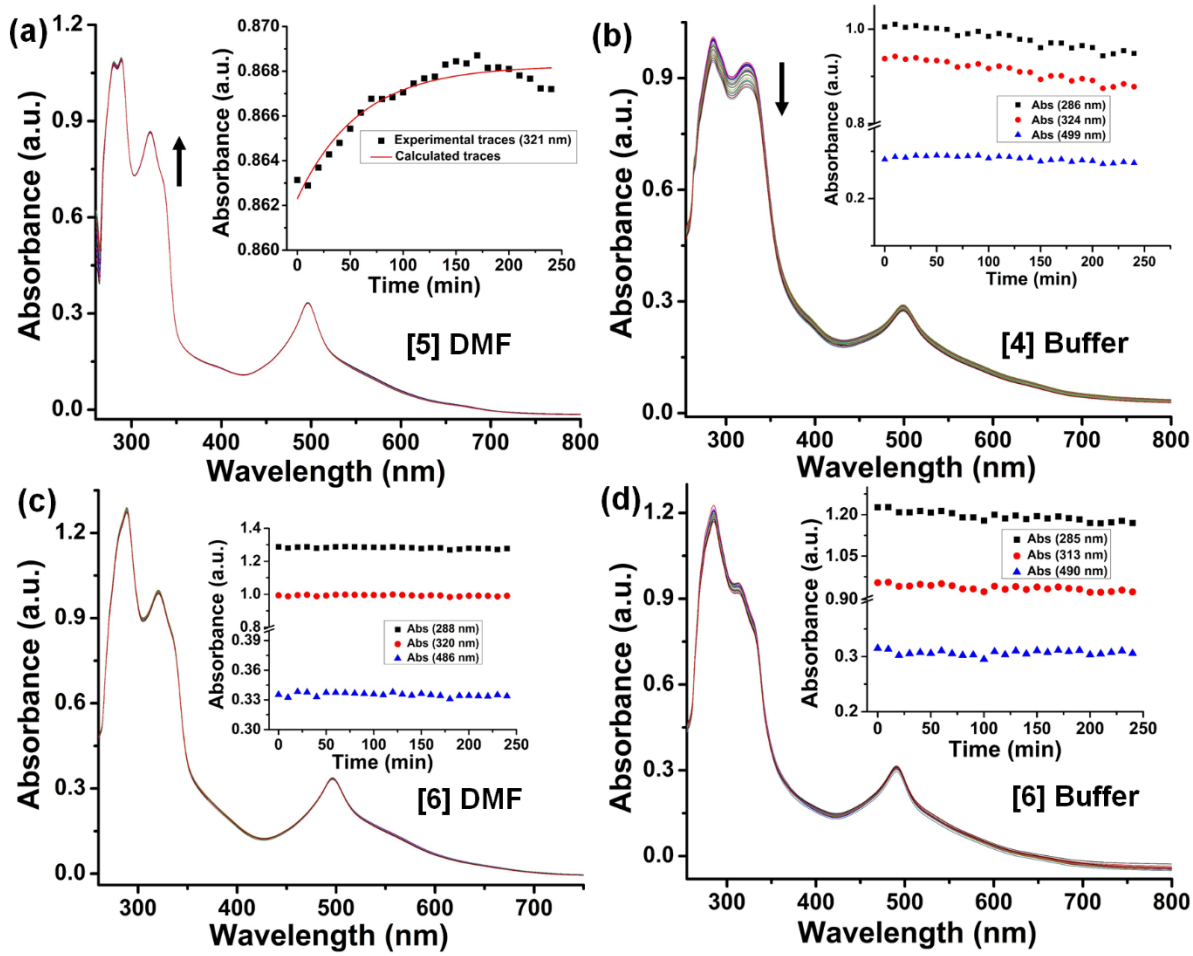

Fig. S16. Solvolysis of the complexes in DMF and in 2% (v/v) DMF–5 mM Tris-HCl/NaCl buffer (pH = 7.2) evident from concomitant changes in absorbance spectral profile at T = 298 K for 4 h. (a) **5** (49 μM) in DMF; (b) **4** (39 μM) in DMF–buffer; (c) **6** (29 μM) in DMF and (d) **6** (29 μM) in DMF–buffer.

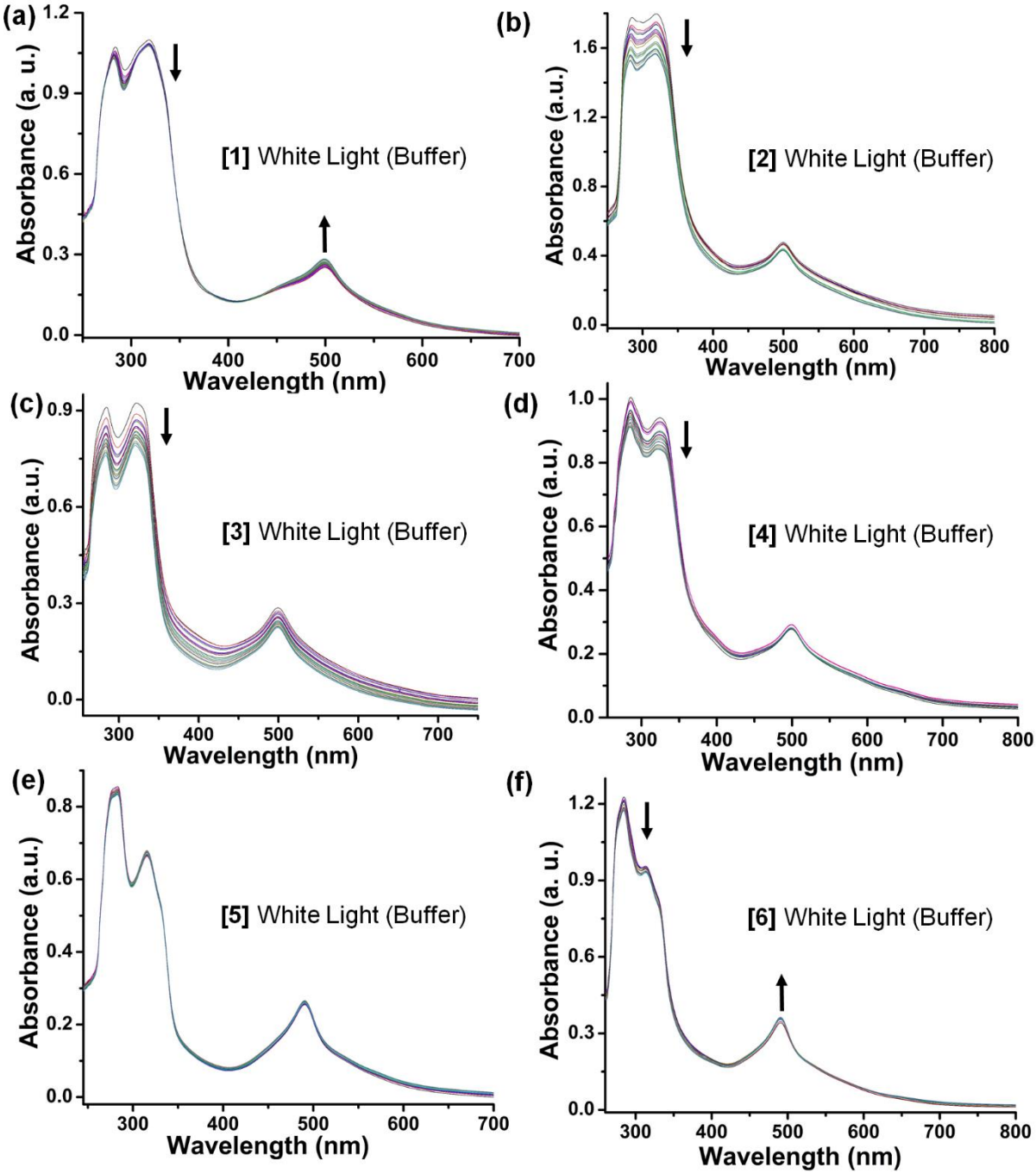

Fig. S17. Photoirradiation of white light (λ_{exc} > 400 nm) to the complexes (a) **1** (58 μM); (b) **2** (39 μM); (c) **3** (39 μM); (d) **4** (39 μM); (e) **5** (39 μM) and (f) **6** (29 μM) for the 0–100 min in 2 % (v/v) DMF–5 mM Tris-HCl/NaCl buffer (pH = 7.2) mixture. T = 298 K.

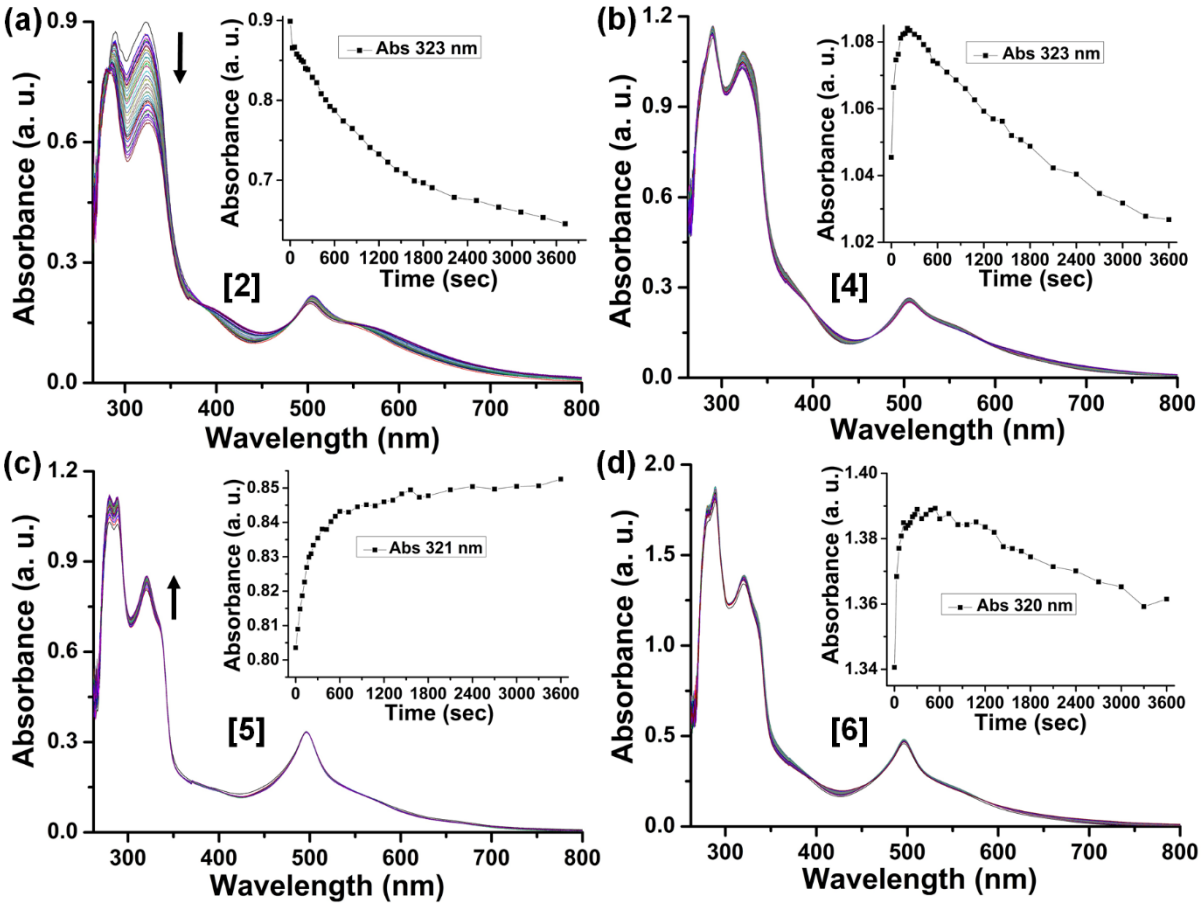

Fig. S18. Green light (λ_{exc} = 530 nm, 3V, 158 lm @ 700mA) induced changes in absorption spectral traces of the complexes in DMF for the period of 0–60 min. (a) **2** (20 μM), inset: Changes in $A_{323\ nm}$ upon photoirradiation; (b) **4** (39 μM), inset: Changes in $A_{323\ nm}$ upon photoirradiation; (c) **5** (39 μM), inset: Changes in $A_{321\ nm}$ upon photoirradiation and (d) **6** (39 μM)**,** inset: Changes in $A_{320\ nm}$ upon photoirradiation.

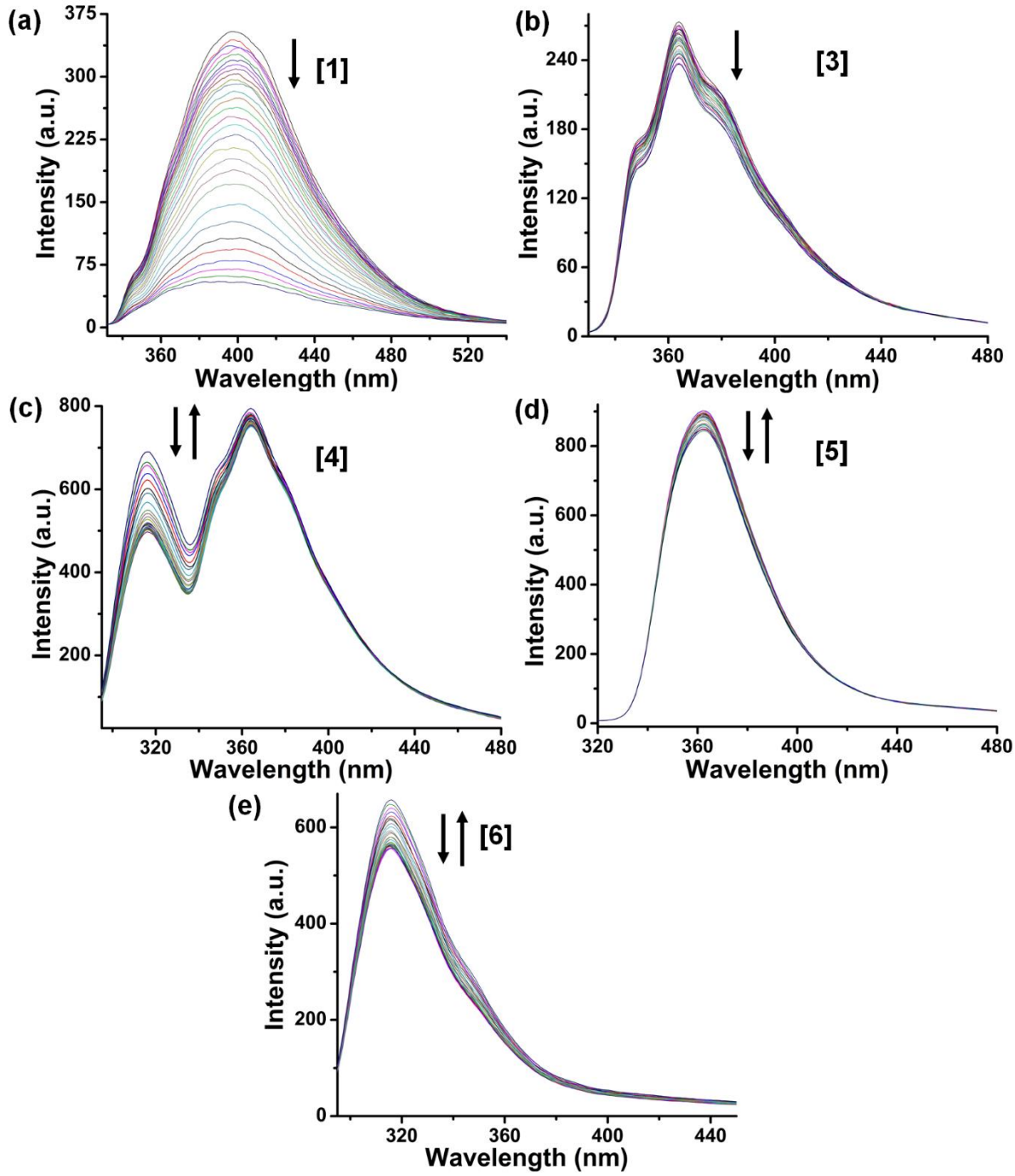

Fig. S19. Green light (λ_{exc} = 530 nm, 3V, 158 lm @ 700mA) induced changes in emission spectral traces of the complexes (20 μM) in DMF, (a) **1**; (b) **3**; (c) **4**; (d) **5** and (e) **6** for the period of 0–60 min.

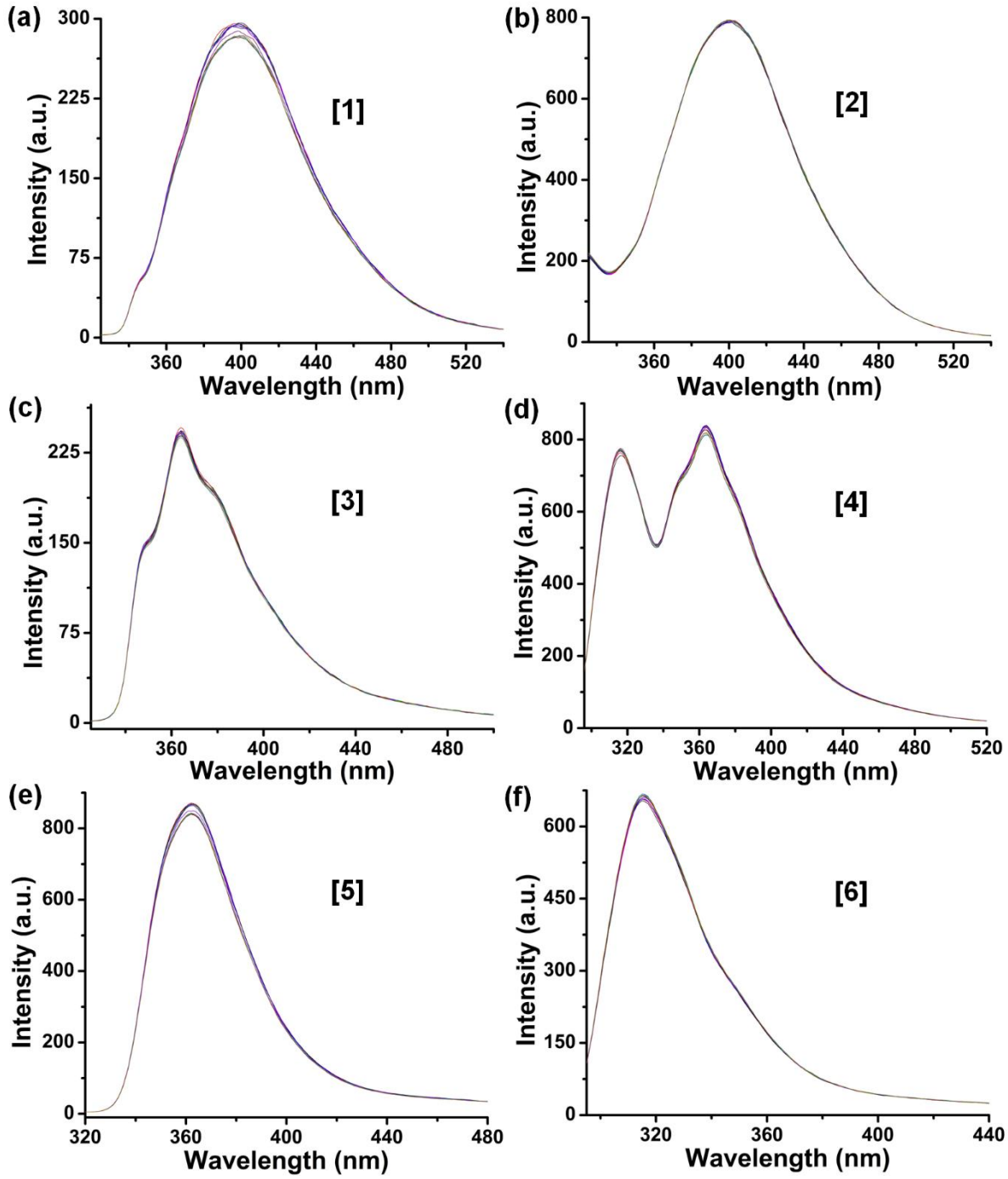

Fig. S20. Time-dependent fluorescence monitoring of the complexes **1**–**6** (20 μM) in dark for 0–60 min in DMF.

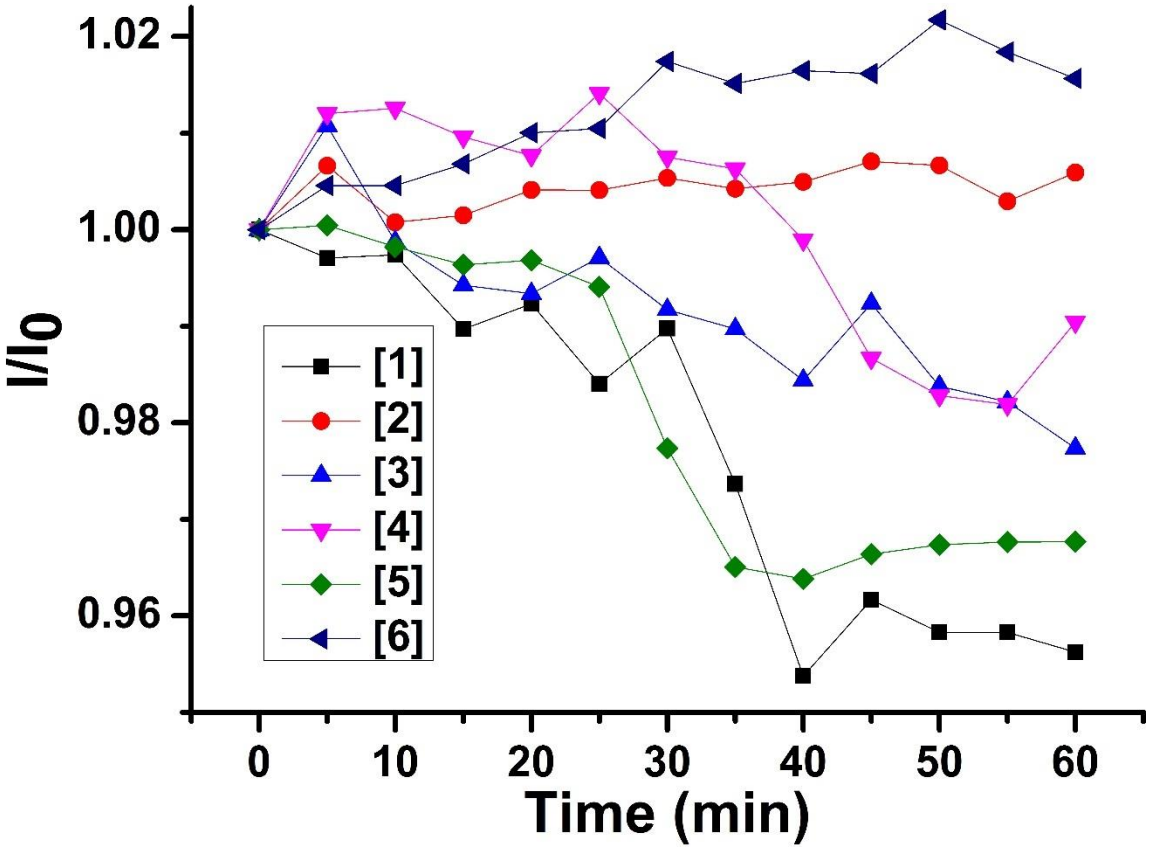

Fig. S21. An overlay of relative changes of fluorescence intensity for 0–60 min of the complexes **1**–**6** (20 μM) in DMF studied in the dark.

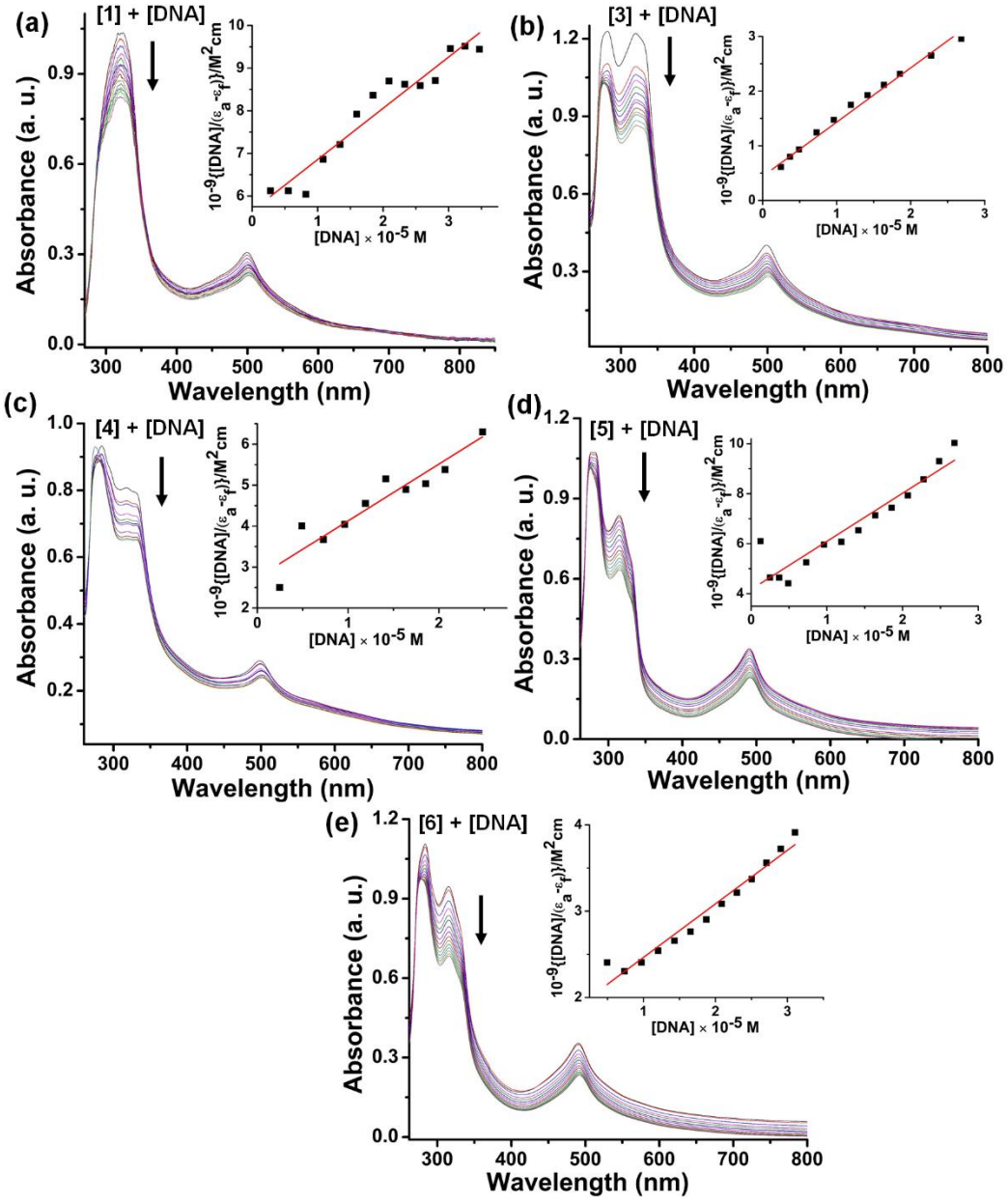

Fig. S22. Binding of the complexes with calf thymus (CT)-DNA. The absorption spectral traces of the complex showing hypochromic and bathochromic shifts in 1% (v/v) DMF–5 mM Tris-HCl/NaCl buffer (pH = 7.2). (a) **1** (58 μM) upon the addition of CT-DNA (0–35 μM); (b) **3** (39 μM) upon the addition of CT-DNA (0–27 μM); (c) **4** (39 μM) upon the addition of CT-DNA (0–25 μM); (d) **5** (39 μM) upon the addition of CT-DNA (0–27 μM); (e) **6** (20 μM) upon the addition of CT-DNA (0–31 μM); Insets: Determination of intrinsic equilibrium binding constant (K_b) from slope to intercept ratio of linear fit of the plot.

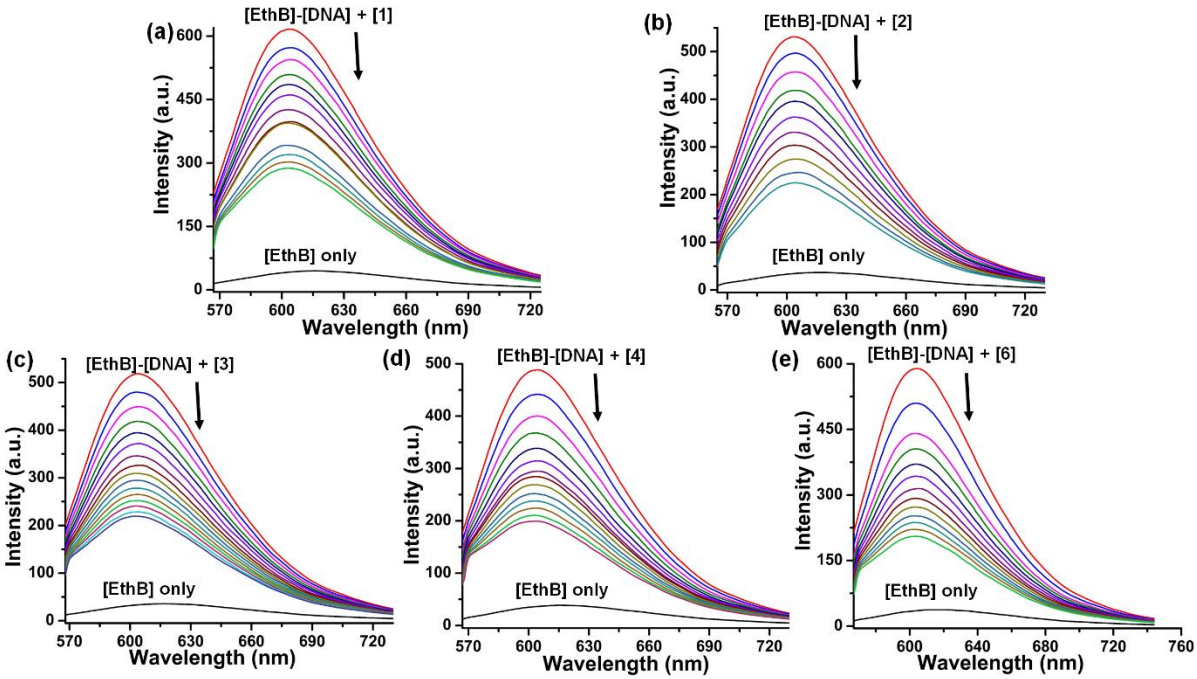

Fig. S23. Quenching of fluorescence emission of ethidium bromide (EthB, 12 μM)-CT DNA (14.4 μM) adduct at ~604 nm in 1% (v/v) DMF–5 mM Tris-HCl/NaCl buffer (pH = 7.2) upon addition of (a) Complex **1** (0–22 μM); (b) Complex **2** (0–19 μM); (c) Complex **3** (0–28 μM); (d) Complex **4** (0–22 μM) and (e) Complex **1** (0–13 μM) showing displacement of EthB and intercalation with DNA.

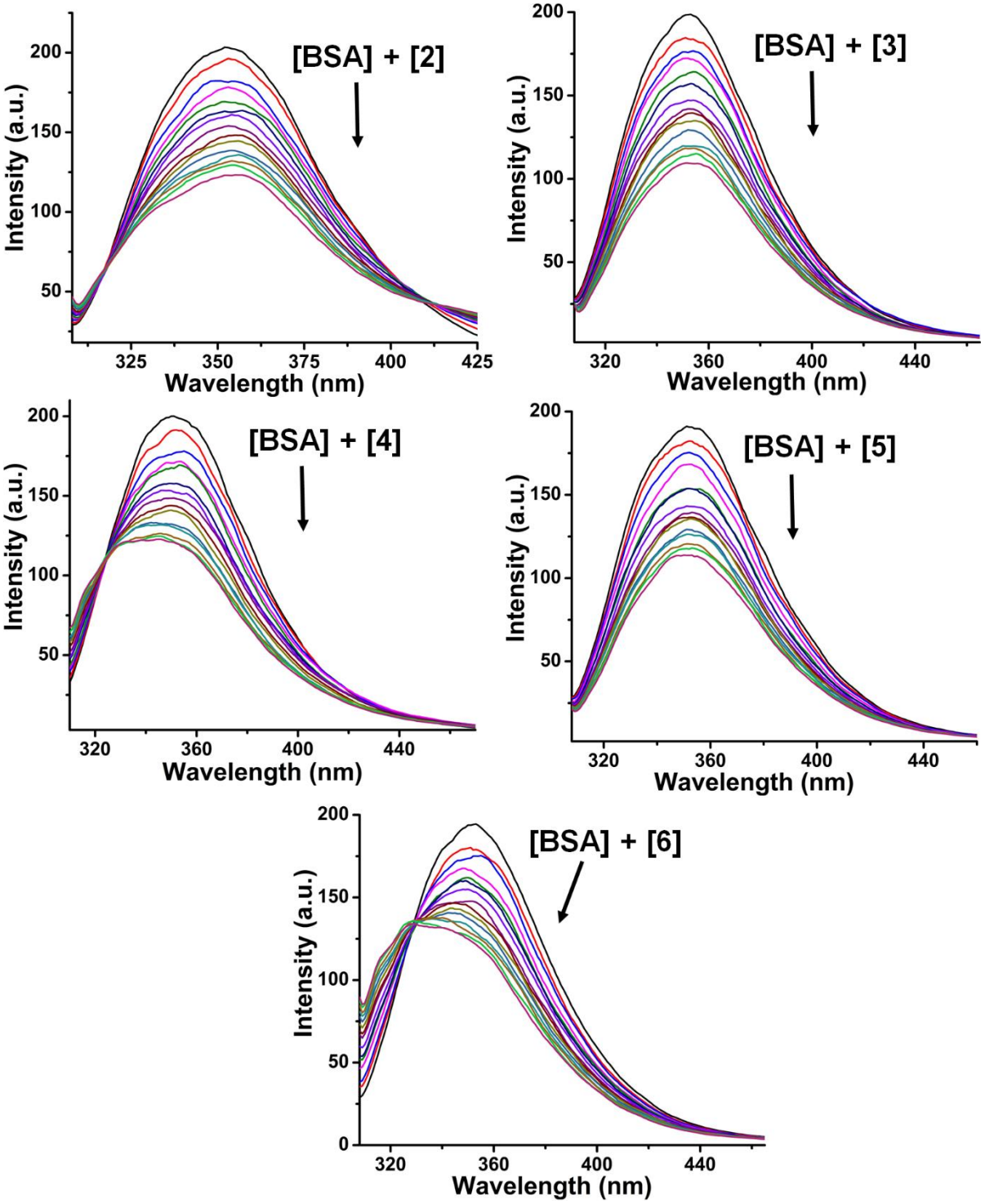

Fig. S24. Bovine serum albumin (BSA) binding of the complexes in 0.7% (v/v) DMF–5mM Tris HCl/NaCl (pH = 7.2) buffer. Fluorescence (λ_{ex} = 295 nm) quenching of the BSA (2 μM) in the presence of increasing complexes **2**–**6** (0–3.5 μM).

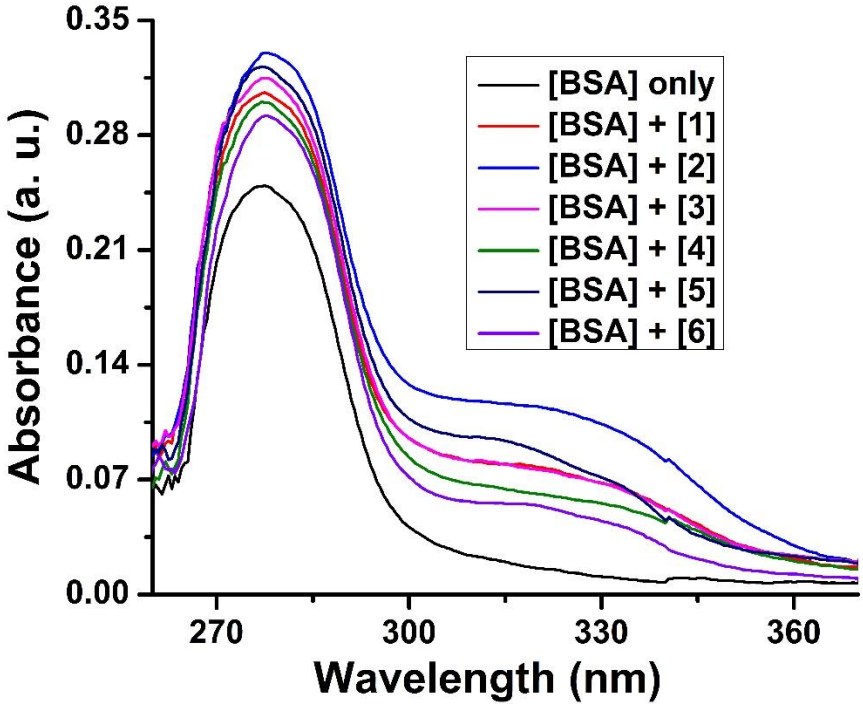

Fig. S25. The absorption spectral overlay of bovine serum albumin (5 μM) and changes upon addition of complexes **1**–**6** (1.5 μM) in in 0.2% (v/v) DMF-5 mM Tris HCl/NaCl (pH = 7.2) buffer.

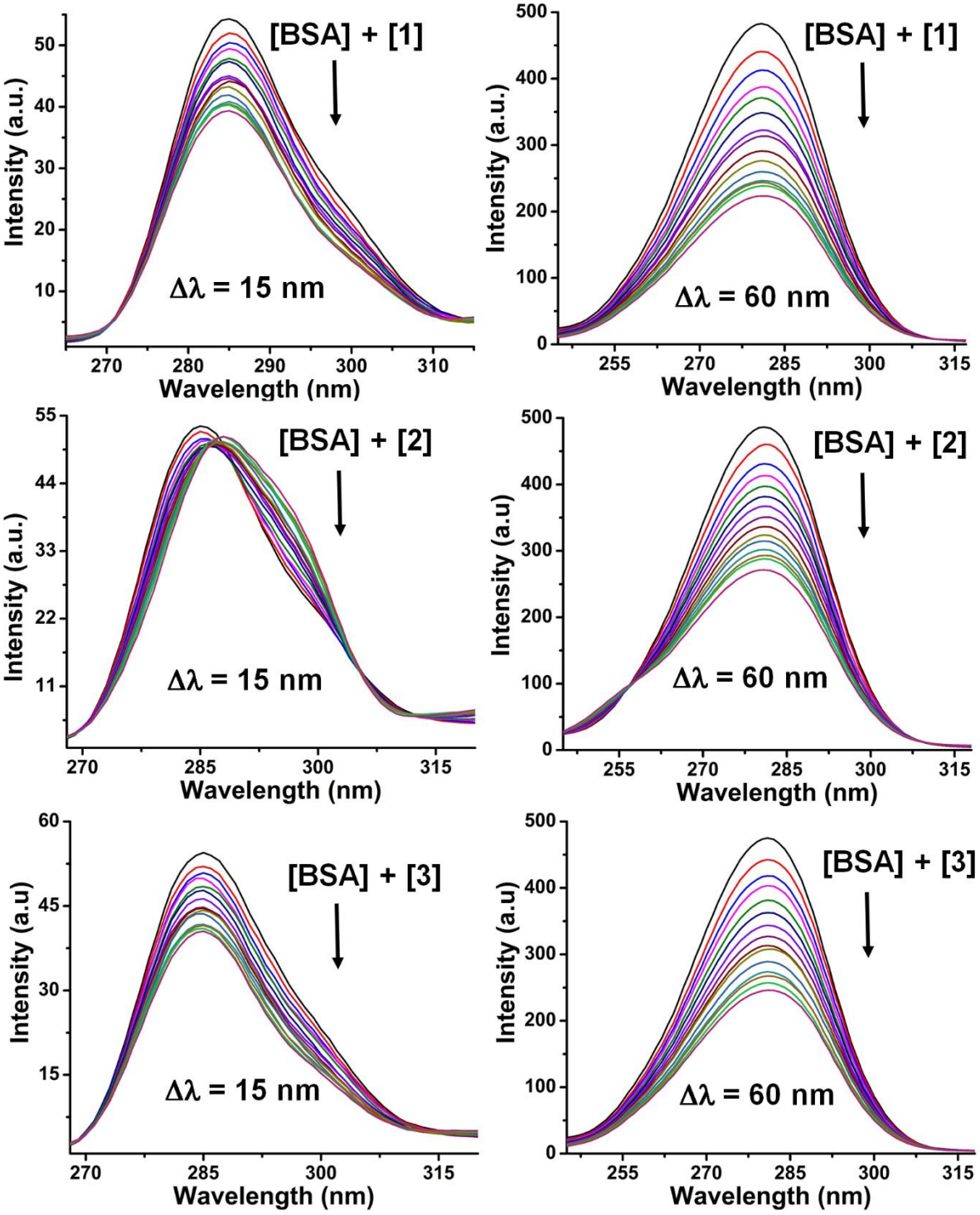

Fig. S26. Bovine serum albumin (BSA) binding of the complexes in 0.7% (v/v) DMF–5mM Tris HCl/NaCl (pH = 7.2) buffer. Synchronous fluorescence with $\Delta\lambda$ = 15 nm and $\Delta\lambda$ = 60 nm of the BSA (2 μM) in the presence of increasing complexes **1**–**3** (0–3.5 μM).

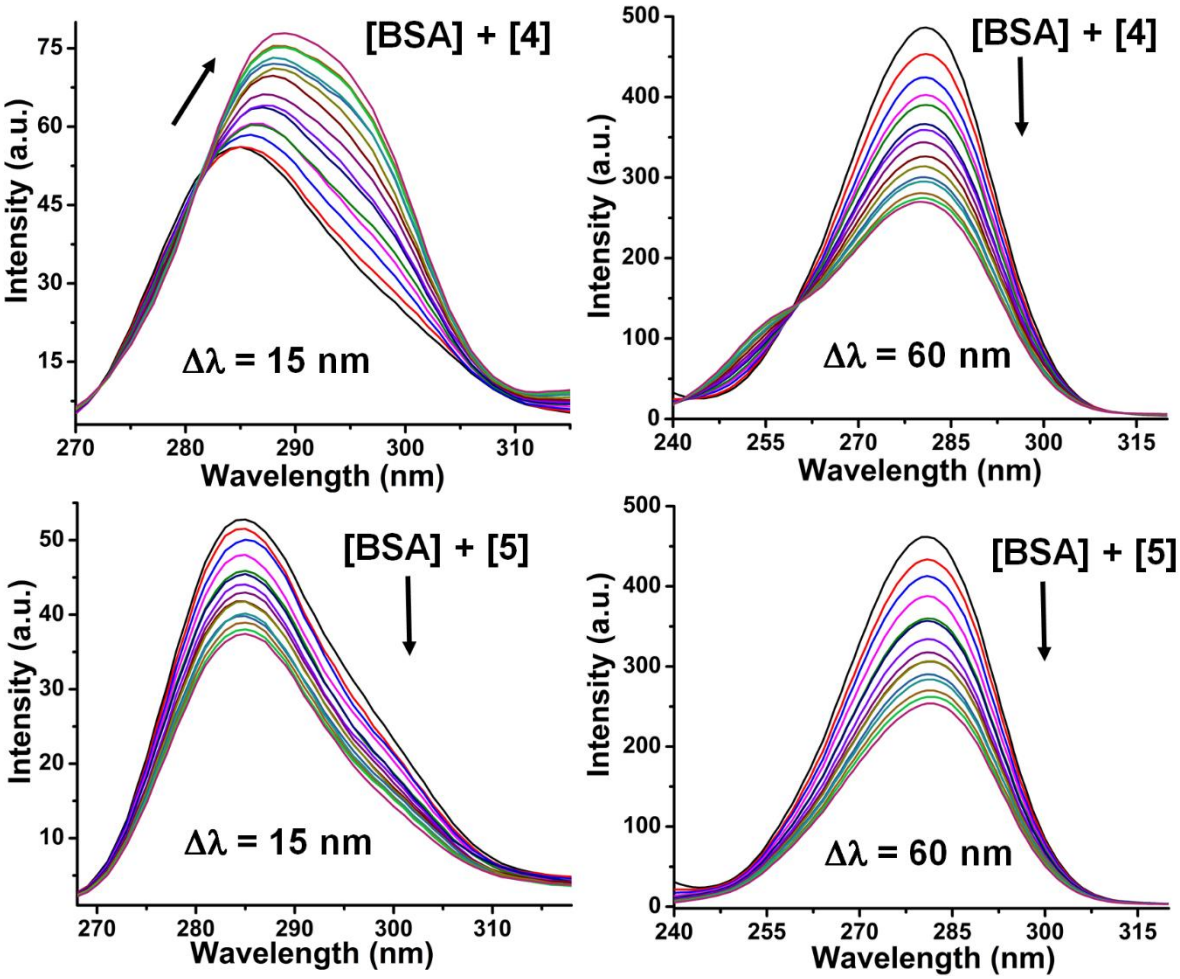

Fig. S27. Bovine serum albumin (BSA) binding of the complexes in 0.7% (v/v) DMF–5mM Tris HCl/NaCl (pH = 7.2) buffer. Synchronous fluorescence with $\Delta\lambda$ = 15 nm and $\Delta\lambda$ = 60 nm of the BSA (2 μM) in the presence of increasing complexes **4** and **5** (0–3.5 μM).

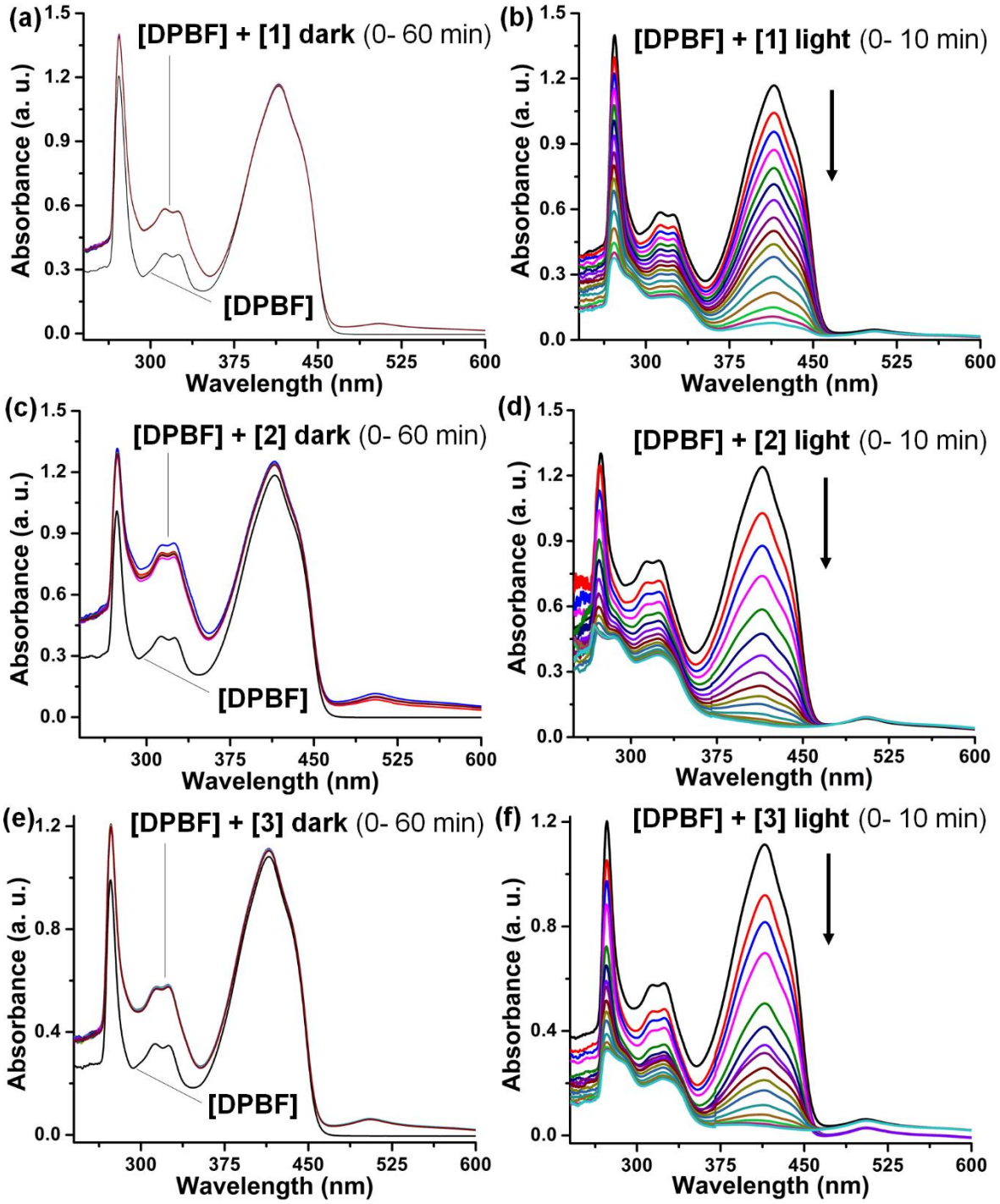

Fig. S28. (a), (c) and (e) absorption spectral profile of mixture of DPBF (50 μM) and complexes **1**, **2**, and **3** (10 μM) respectively in the dark for 0–60 mins. (b), (d) and (f) green light (λ_{ex} = 530 nm) induced absorption spectral changes of mixture of DPBF (50 μM) and complexes **1**, **2** and **3** (10 μM) for 0–10 mins.

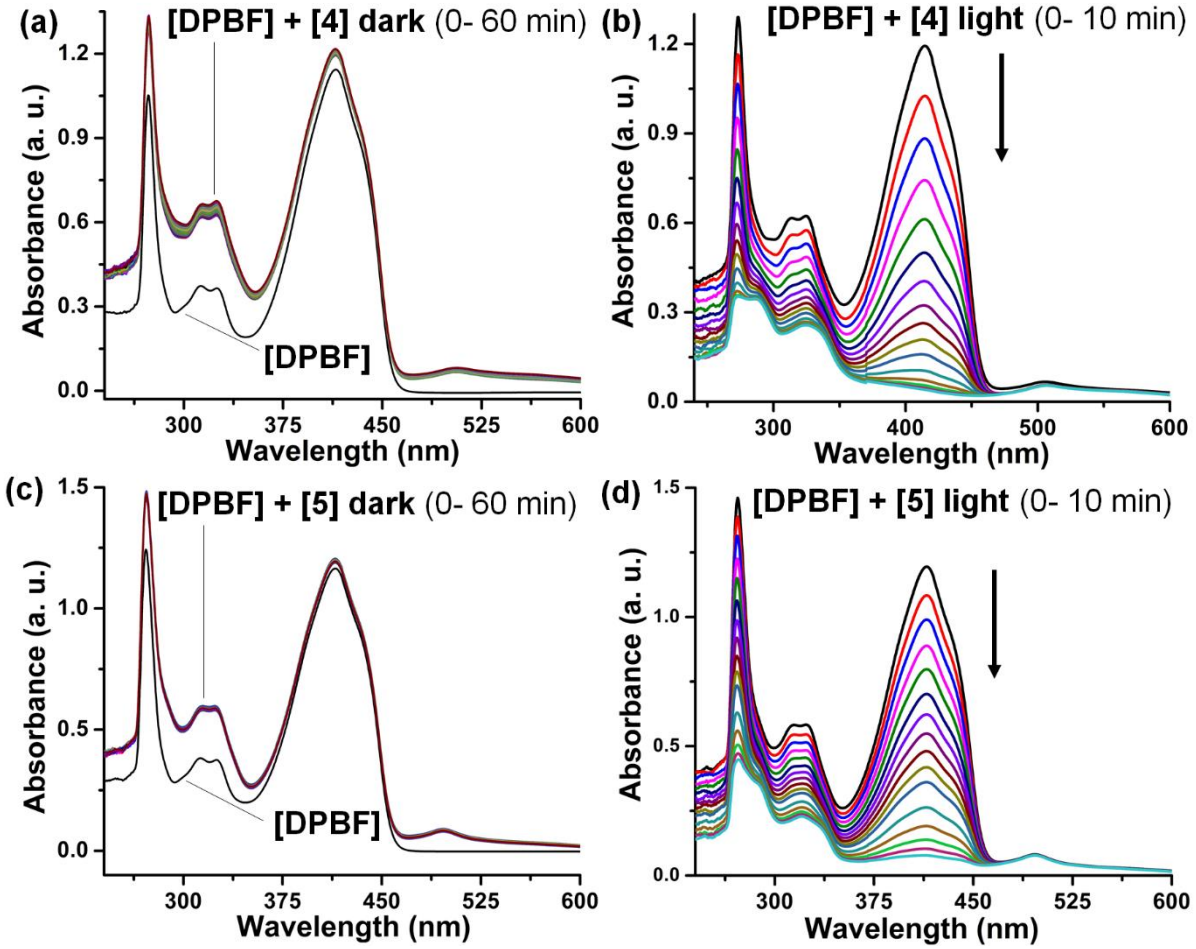

Fig. S29. (a) and (c) absorption spectral profile of mixture of DPBF (50 μM) and complexes **4** and **5** (10 μM) respectively in the dark for 0–60 mins. (b) and (d) green light (λ_{ex} = 530 nm) induced absorption spectral changes of mixture of DPBF (50 μM) and complexes **4** and **5** (10 μM) for 0–10 mins.

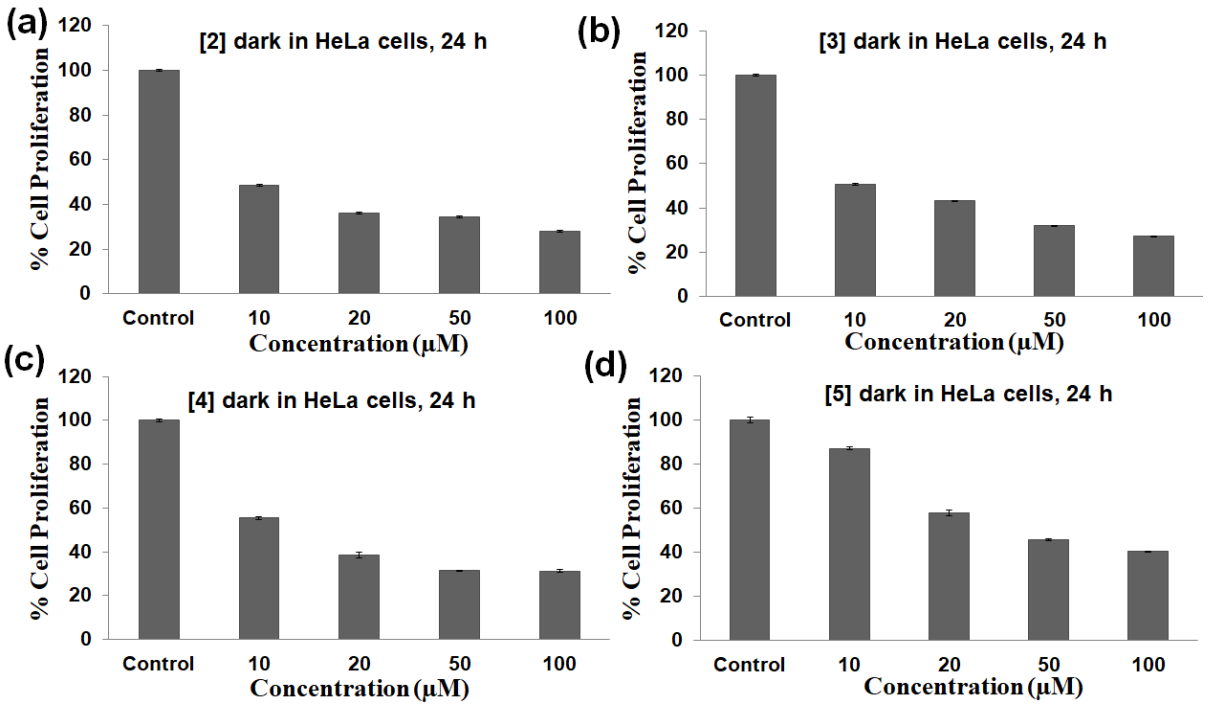

Fig. S30. Dose-dependent cytotoxicity of the complexes **2–5** in the dark after 24h incubation in HeLa cells determined from MTT assay.

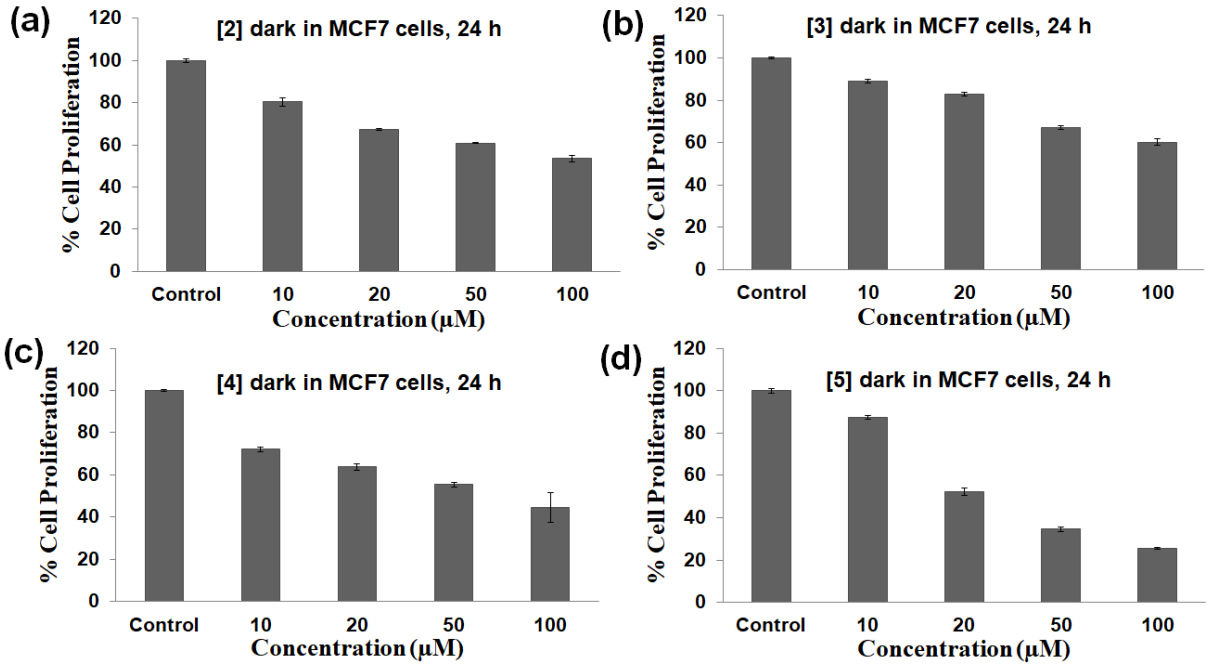

Fig. S31. Dose-dependent cytotoxicity of the complexes **2–5** in dark after 24 h incubation in MCF7 cells determined from MTT assay.

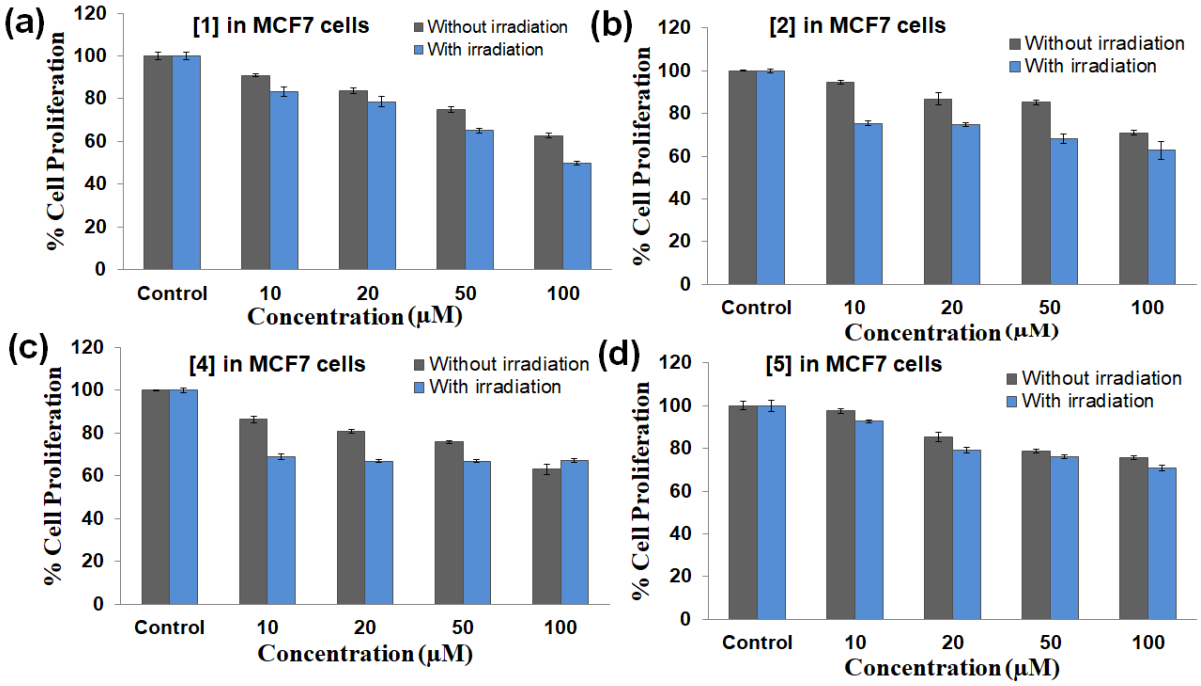

Fig. S32. Dose-dependent cytotoxicity of the complexes **1**, **2**, **4**, and **5** in the dark and upon irradiation with low energy UV-A light of 365 nm in MCF7 cells determined from MTT assay. Incubation time with complexes = 4 h and irradiation time = 1 h.

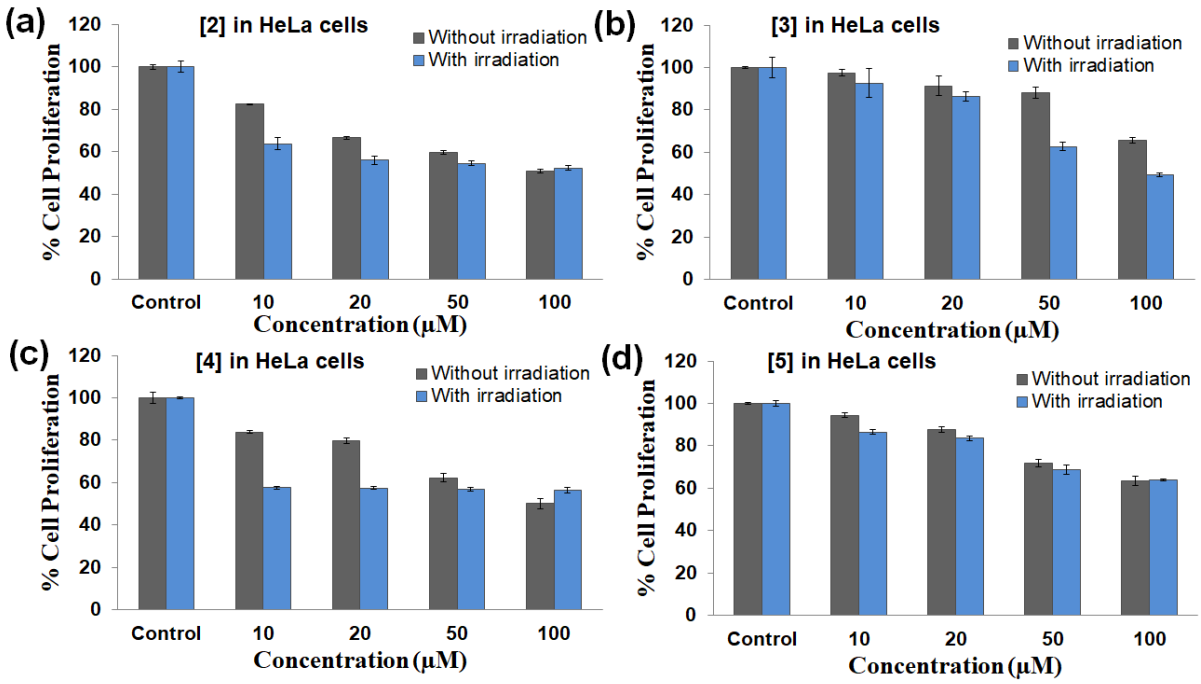

Fig. S33. Dose-dependent cytotoxicity of the complexes **2–5** in the dark and upon irradiation with low energy UV-A light of 365 nm in HeLa cells determined from MTT assay. Incubation time with complexes = 4 h and irradiation time = 1 h.

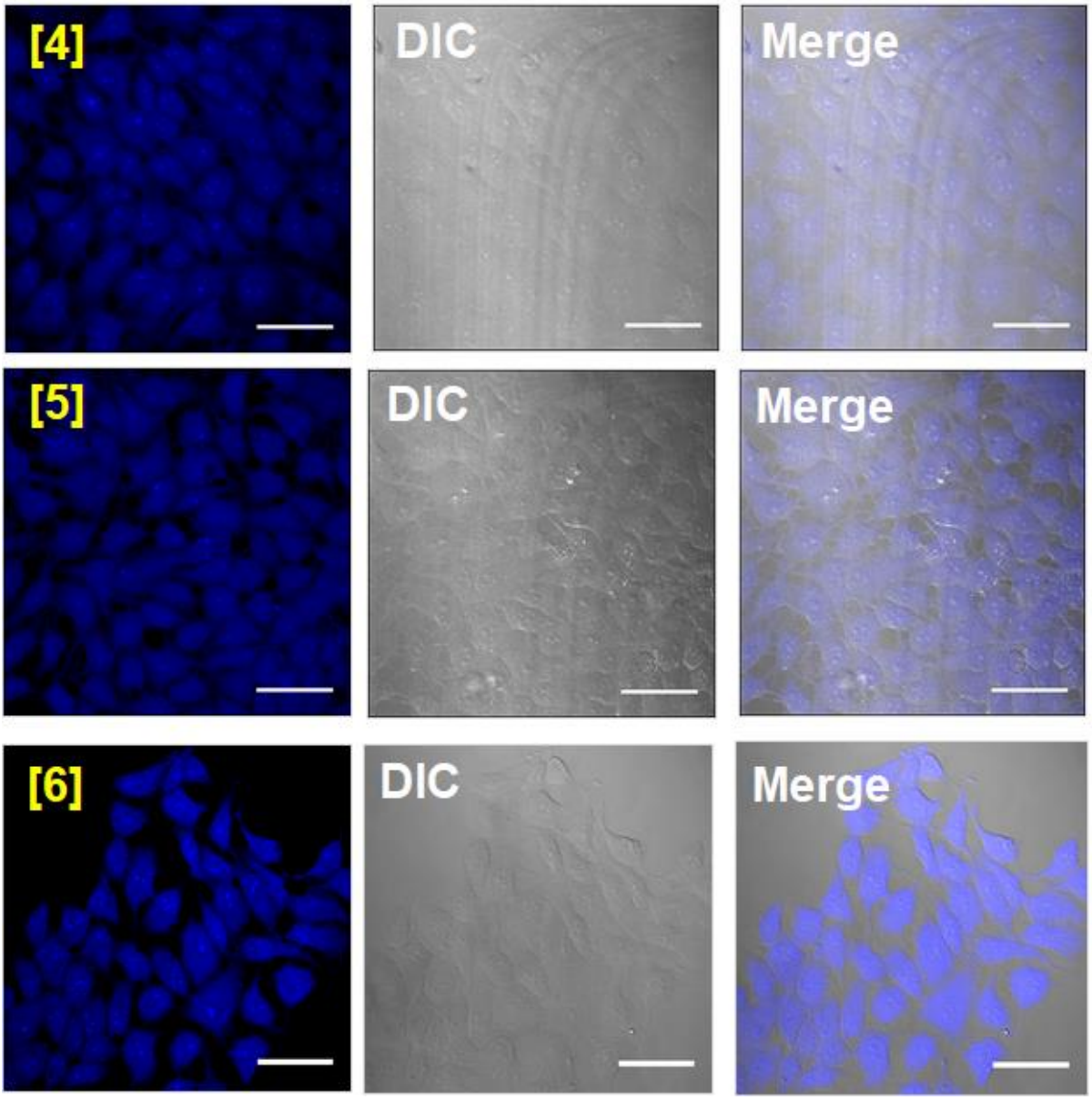

Fig. S34. CLSM images demonstrating uptake of the complexes **4**, **5**, and **6** (10 μM) in MCF7 cells after 4h incubation. The excitation and emission wavelengths of complexes were 350 nm and 460 nm, respectively. Scale bar-50 µm.

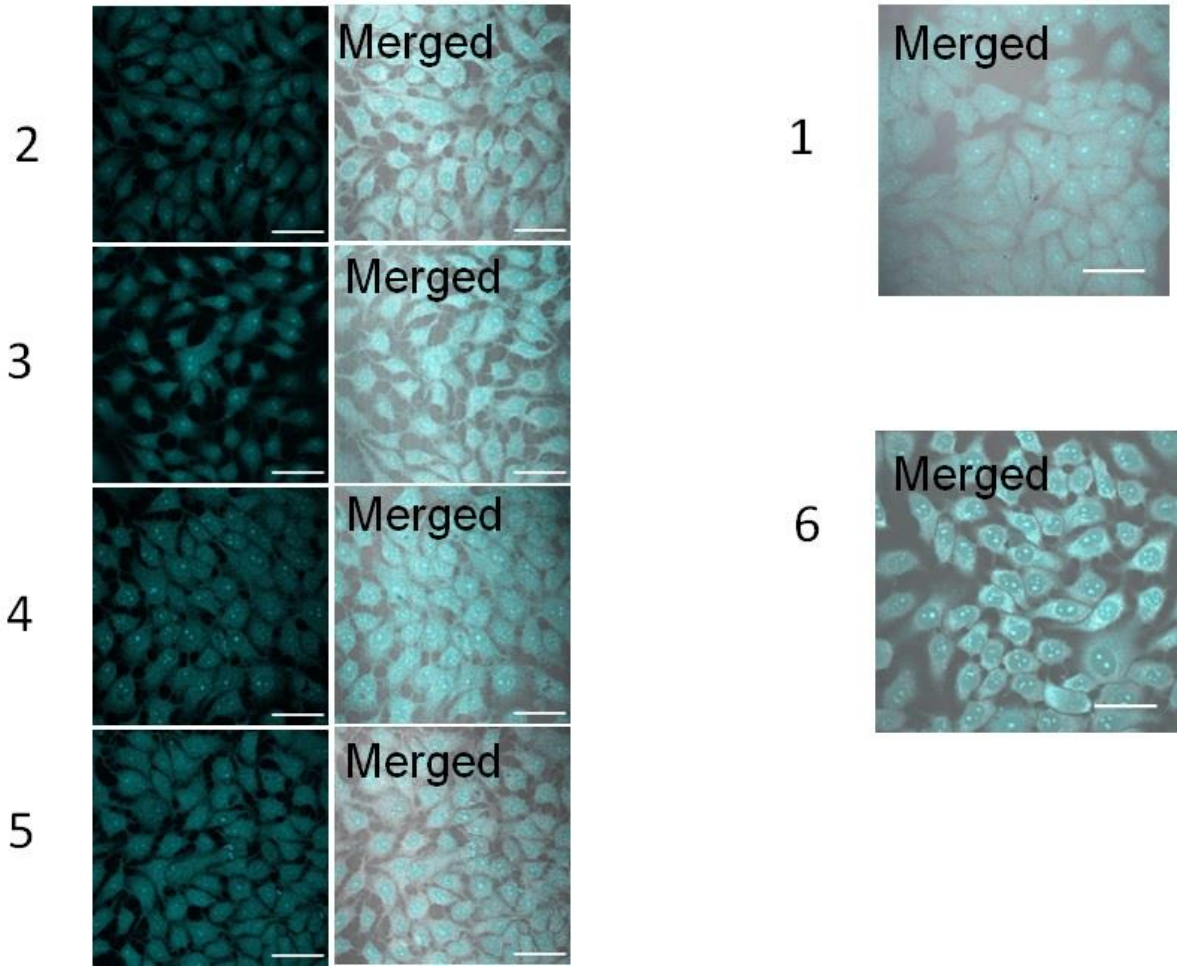

Fig. S35. The confocal laser scanning microscopic (CLSM) images demonstrating uptake of the complexes **1**–**6** (10 µM) in MCF7 cells after 4h incubation. The excitation and emission wavelengths are 350 nm and 460 nm, respectively, cyan pseudo color was given to incorporate better contrast. Scale bar-50 µm.

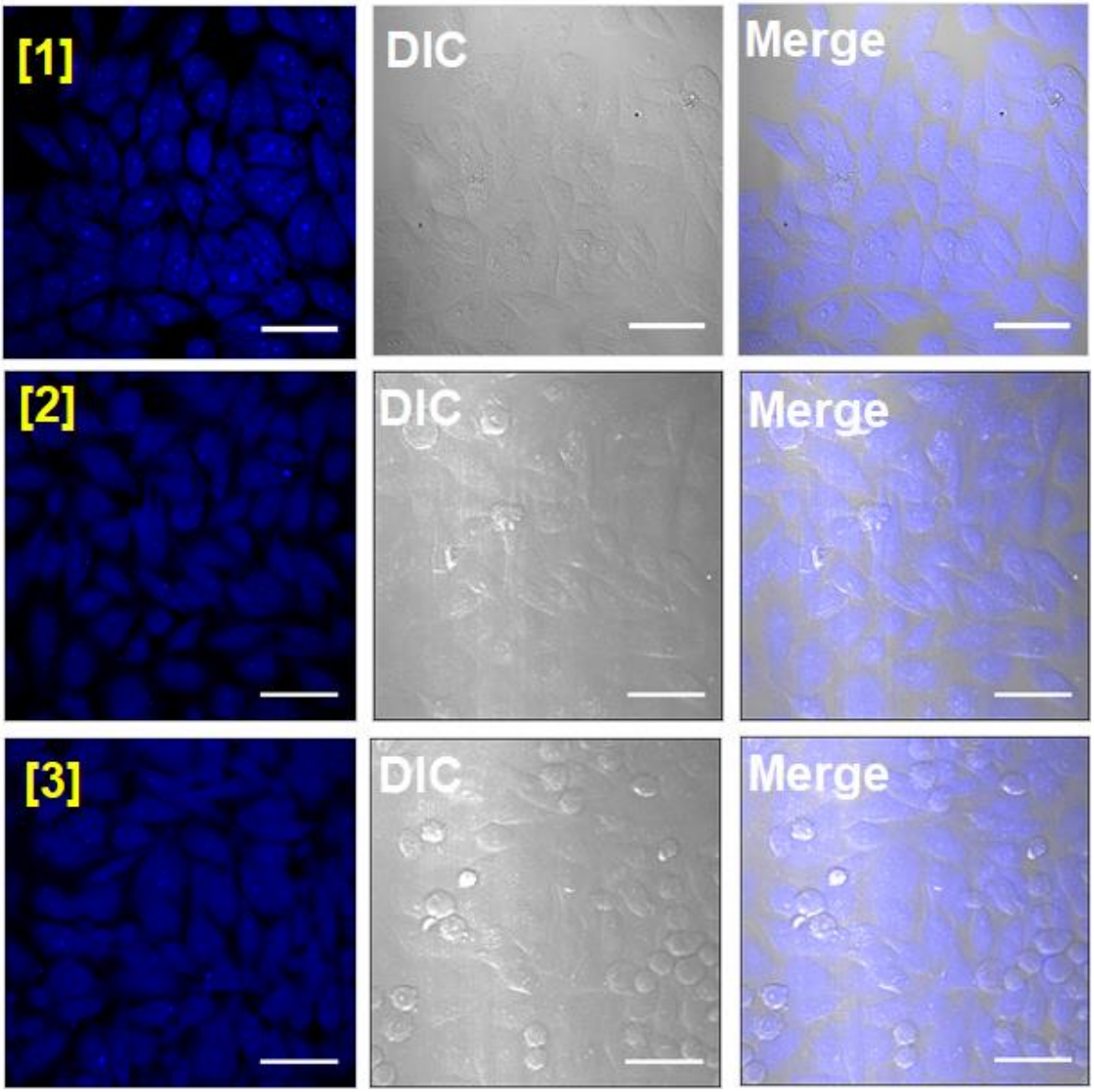

Fig. S36. CLSM images demonstrating uptake of the complexes **1**–**3** (10 μM) in HeLa cells after 4h incubation. The excitation and emission wavelengths of complexes were 350 nm and 460 nm, respectively. Scale bar- 50 µm.

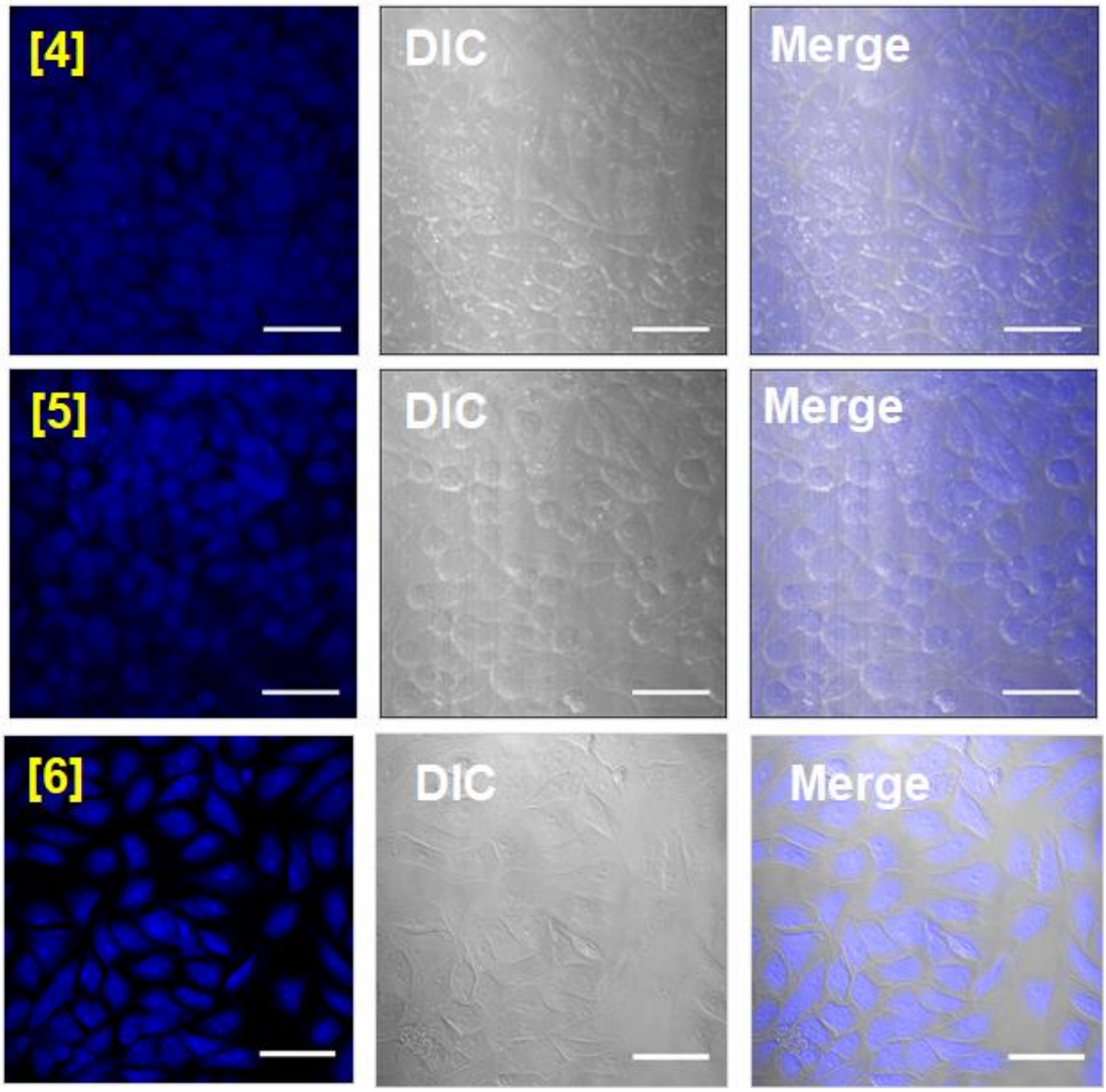

Fig. S37. CLSM images demonstrating uptake of the complexes **4–6** (10 μM) in HeLa cells after incubation 4h. The excitation and emission wavelengths of complexes were 350 nm and 460 nm, respectively. Scale bar- 50 µm.

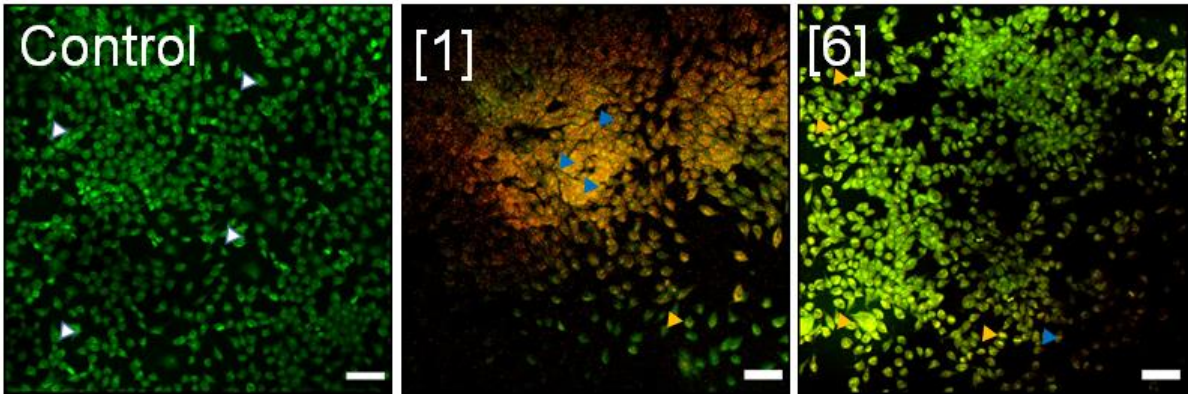

Fig. S38. Cell apoptosis detection by acridine orange (AO) and ethidium bromide (EthB) (100 μg/mL) dual staining in MCF7 cell lines incubated with complexes **1** and **6** (10 μM) for 24 h. Untreated breast cancer cells stained in green homogenously demonstrate normal morphology (white arrow), early apoptosis is observed in yellow as chromatin condensation (yellow arrow), and late apoptosis is observed as yellow/orange color with characteristic nuclear fragmentation and blebbing (blue arrow). Scale bar-100 μm.